Science of the Total Environment 857 (2023) 158833

Contents lists available at ScienceDirect

Science of the Total Environment

journal homepage: www.elsevier.com/locate/scitotenv

Tracking of sea level impact on Caspian Ramsar sites and potential restoration of the Gorgan Bay on the southeast Caspian coast

Hamid A.K. Lahijani [a,b,*], Jafar Azizpour [a], Klaus Arpe [c,1], Behrooz Abtahi [d], Reza Rahnama [a], Parvin Ghafarian [a], Mohammad Ali Hamzeh [a], Ali Hamzehpour [a], Mohammadreza Mohammadpour Penchah [e], Seyed Masoud Mahmoudof [a]

[a] Iranian National Institute for Oceanography and Atmospheric Science, Tehran 14118-13389, Iran
[b] Eurasian Institute of Earth Sciences, Istanbul Technical University (ITU), Maslak, Istanbul 34469, Turkey
[c] Max Planck Institute for Meteorology, Hamburg, Germany
[d] Faculty of Life Sciences and Biotechnology, Shahid Beheshti University, Tehran, Iran
[e] Geophysical Institute, University of Bergen, Norway

HIGHLIGHTS

- Caspian coastal Ramsar sites were mapped over 3 periods of different water levels.
- A recent significant shrinking of coastal wetlands was observed.
- A multidisciplinary approach was applied to the Gorgan Bay: field work and simulations.
- Maintenance of bay inlets will enhance water exchange and quality, otherwise the bay could be a dust source.

GRAPHICAL ABSTRACT

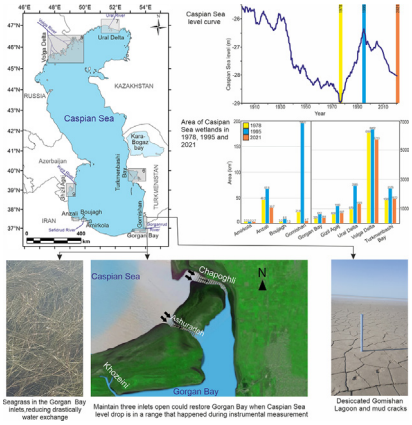

ARTICLE INFO

Editor: Fernando A.L. Pacheco

Keywords:
Coastal wetland
Coastal lagoon
Lake level change
Climate change
Lagoon desiccation

ABSTRACT

The situation of Ramsar sites along the Caspian Sea coast has deteriorated over the past decades, and this is more noticeable in the narrow coastal strip of the south Caspian Sea. In this study we investigate how the Caspian Sea level changes affect the coastal Ramsar sites. Particularly, we focus on the Gorgan Bay in the southeast corner of the Caspian Sea, which is experiencing extensive water level decline, even desiccation. We used satellite images from three periods corresponding to periods of two sea level falls and one sea level rise, in order to decipher spatio-temporal changes of the wetlands. We conducted field campaign in the Gorgan Bay for sampling and measurement of physical, chemical and biological parameters. We simulated water circulation for the past, current and future conditions of the Gorgan Bay, which is essential to sustain better water exchange between the Bay and the Caspian Sea. We applied dust simulation in the case of a total desiccation of the Gorgan Bay. The result shows that the total area of the Caspian coastal Ramsar sites during the two periods of the sea level fall is almost the same; however, the aerial changes in the southern wetlands are more visible. Nutrient and plankton analysis of the Gorgan Bay display mainly mesotrophic conditions, in

Abbreviations: CS, Caspian Sea; CSL, Caspian Sea Level; GB, Gorgan Bay.

* Corresponding author at: Iranian National Institute for Oceanography and Atmospheric Science, Tehran 14118-13389, Iran.
E-mail address: lahijani@inio.ac.ir (H.A.K. Lahijani).

[1] Retired.

http://dx.doi.org/10.1016/j.scitotenv.2022.158833
Received 30 June 2022; Received in revised form 2 September 2022; Accepted 13 September 2022
Available online 16 September 2022

some areas close to eutrophic ones. The average current velocity in the main inlet is 2.5 cms^{-1}. Dust simulation indicates that in case of the Gorgan Bay desiccation, it will become a dust source for the surrounding area up to 60 km. Simulation of the water circulation with dredging of inlets (future scenario), indicates that the water exchange velocity doubles compared to the current scenario. A recommended inlet maintenance would accelerate water circulation and reduce residence time, which will lead to better trophy and prevent bay desiccation.

1. Introduction

Wetlands provide precious facilities for human life, fauna and flora including habitats for numerous species, and space for recreation and tourism. Moreover, wetland preservation has an impact on climate (Janse et al., 2019; Narayan et al., 2017; Xu et al., 2020). On the contrary, they have a very sensitive response to climate change and human activities (Derolez et al., 2020; Lefebvre et al., 2019; Barale, 2008). Pollution, eutrophication, area reduction during inundation by squeezing against fixed coastal infrastructure, desiccation and human intervention are prominent issues that the world wetlands are currently challenging (Kopelevich et al., 2004; Karydis, 2009; Wu et al., 2022). Global climate change leads to rapid sea level rise that have adverse impacts on coastal wetlands (Spencer et al., 2016; Grenfell et al., 2016). By the end of the current century, world wetlands will lose significant part of the area and this is associated with a reduction in biodiversity and ecosystem services (Fan et al., 2021; Reed et al., 2020). In contrast to the world sea level rise, many inland basins encounter water level fall and wetland desiccation (Gaybullaev et al., 2012; Sharifi et al., 2018; Prange et al., 2020) that enhanced dust emission in the arid and semiarid regions (Zucca et al., 2021; Rashki et al., 2021; Xi and Sokolik, 2016).

Intensive pressure on both oceanic and inland coastal wetlands causes wetland degradation that require substantial attention for protection and management (Fan et al., 2021; Liu et al., 2020; Miloshis and Fairfield, 2015). Mitigation and restoration measures are important actions to address the issues at the root of wetland degradation (Eagle et al., 2022; Martin et al., 2022; Yuan et al., 2022). The main goal of restoration is to assist natural processes acting in the wetlands with the aim of recovering their basic ecological functions. Enhancing wetlands area, depth and water quality are key components that help - recovering their biological diversity and ecosystem services (Steyer and Llewellyn, 2000; Zhang et al., 2021).

Ramsar wetlands currently encompass 2412 ecosystems that have international importance for conservation (Ramsar List, 2021). The Convention on Wetlands was adopted in the Ramsar city, Caspian Sea (CS) coast, which comprises now ten coastal wetlands enlisted in the Convention (Table S1, Fig. 1; An Introduction to the Convention on Wetlands, 2016). The CS coastal wetlands currently encounter drastic shrinking and desiccation due to rapid sea level fall and mismanagement of water resources (Khorami Pour et al., 2015; Leummens, 2018). The Caspian coastal wetlands that are located on the CS shores benefit from the CS waters. They are mainly river mouths, beaches, coastal lagoons, and bays, the extent of which is strongly dependent on Caspian Sea level (CSL) (Kroonenberg et al., 2000), which dropped around 1.9 m during the past two decades (https://ipad.fas.usda.gov/cropexplorer/global_reservoir/). The Caspian coastal bays and lagoons have experienced reductions during the sea level fall of the 1960s and 1970s; however, the current anthropogenic pressure and climate change is superimposed on the impact of sea level fall (Fig. 2) and exacerbates ecosystem decline. Many investigations have been devoted to the different aspects of CSL change. CSL changes in the past (Varushenko et al., 1987; Rychagov, 1997; Lahijani et al., 2009; Naderi Beni et al., 2013; Kakroodi et al., 2015; Leroy et al., 2022a), role of human activities on CSL changes (Mikhailov, 1997; Demin, 2007; Lahijani et al., 2008; Akhmadiyeva and Abdullaev, 2019), impact of CSL on coastal areas (Kroonenberg et al., 2000; Naderi Beni et al., 2013) and forecast of CSL (Elguindi and Giorgi, 2006; Arpe and Leroy, 2007; Renssen et al., 2007; Arpe et al., 2013; Koriche et al., 2021) are the main topics that have previously been focused on. However, the impact of CSL changes on Caspian Ramsar wetlands and how CSL rise and fall affect these wetland loss and gain has so far attracted little attention.

Gorgan Bay (GB) in the southeast corner of the CS, which is separated from the sea by the Miankaleh Spit, and its western appendix known as Lapoo-Zaghmarz (Figs. 1 and 3) were designated Ramsar sites in 1975 (Ramsar List, 2020). The GB is a shallow (around 2 m depth) basin that was connected to the CS through two inlets during the CS high stand (1980–2010) (Kakroodi et al., 2012), one of which desiccated by the falling sea level and the other one was divided into two inlets, with an emerging island between them. In the very shallow inlets, seagrass)*Ruppia maritima* (is growing, which significantly reduces water exchange between the GB and CS. The GB and adjacent environments including Miankaleh Spit and Lapoo-Zaghmarz wetland are the hosts for migratory birds and are a wildlife refuge (Vazin, 2021). The southern part of the GB, densely populated, is extensively used for agriculture, from which nutrients are delivered to the GB. Intensive human activities and sea level fall are all attributed to the reduction in water depth and volume, water exchange and surface area of the GB as well as causing eutrophication and anoxia in some parts (Maleki et al., 2020; Aali and Shahryari, 2021). It is known that, in the past, the area of the GB has fluctuated widely from desiccation to full connection to the CS (Leroy et al., 2019, Leroy et al., 2022c). Despite of the works by scholars and state organizations that were devoted to the various issues of the GB (Ranjbar and Hadjizadeh Zaker, 2016; Gholizadeh and Cera, 2022), studies concerning the preservation of whole ecosystem are missing. The sustainability of the GB requires free connection to the CS, which is essential to preserve the ecosystem under CSL fluctuations in a vertical range that happened during the period of instrumental measurements at least.

In this study, we follow two goals concerning the Caspian coastal Ramsar sites. First, we investigate nine internationally important Caspian coastal wetlands during two periods of CSL fall and one period of rise to unravel wetland loss and gain during the past four decades. To perform this goal, we have used satellite images to map wetland changes. Our second goal in this research is to focus on an important wetland, the GB, that currently suffers from a severe decrease of its area, depth, water quality and connection with the CS. The GB experienced lower CSL during 1970s compared to the current one; however, in the current condition, it displays faster degradation. We proposed that the GB has potential for restoration, but we should assist it to empower self-restoration. To do this, we conducted field measurements, sampling and laboratory analyses, and part of the retrieved data was used for model simulation. We applied dust simulation and simulation of water circulation. Dust simulation is used to show the possible adverse impact on the GB in case of desiccation and whether it plays as source of dust for the region. The simulation of water circulation is necessary to show a likely improvement of the water quality in case of inlet maintenance and better water exchange between the GB and CS. Our findings will shed light on a topic that is not common in the current global warming and sea level rise contexts. The urgency of the CSL fall and its broad impact are not well perceived in the circum-Caspian states, an unfortunate situation that requires pressing awareness and action taking by managers to organize measures for conservation of the Caspian Ramsar sites.

2. Setting

2.1. Caspian Sea

The CS is oriented north to south, with a length of about 1200 km and a width of about 400 km (Fig. 1). The sea surface area (at an altitude of 28 m below world sea level) is about 360,000 km^2, and the volume of water

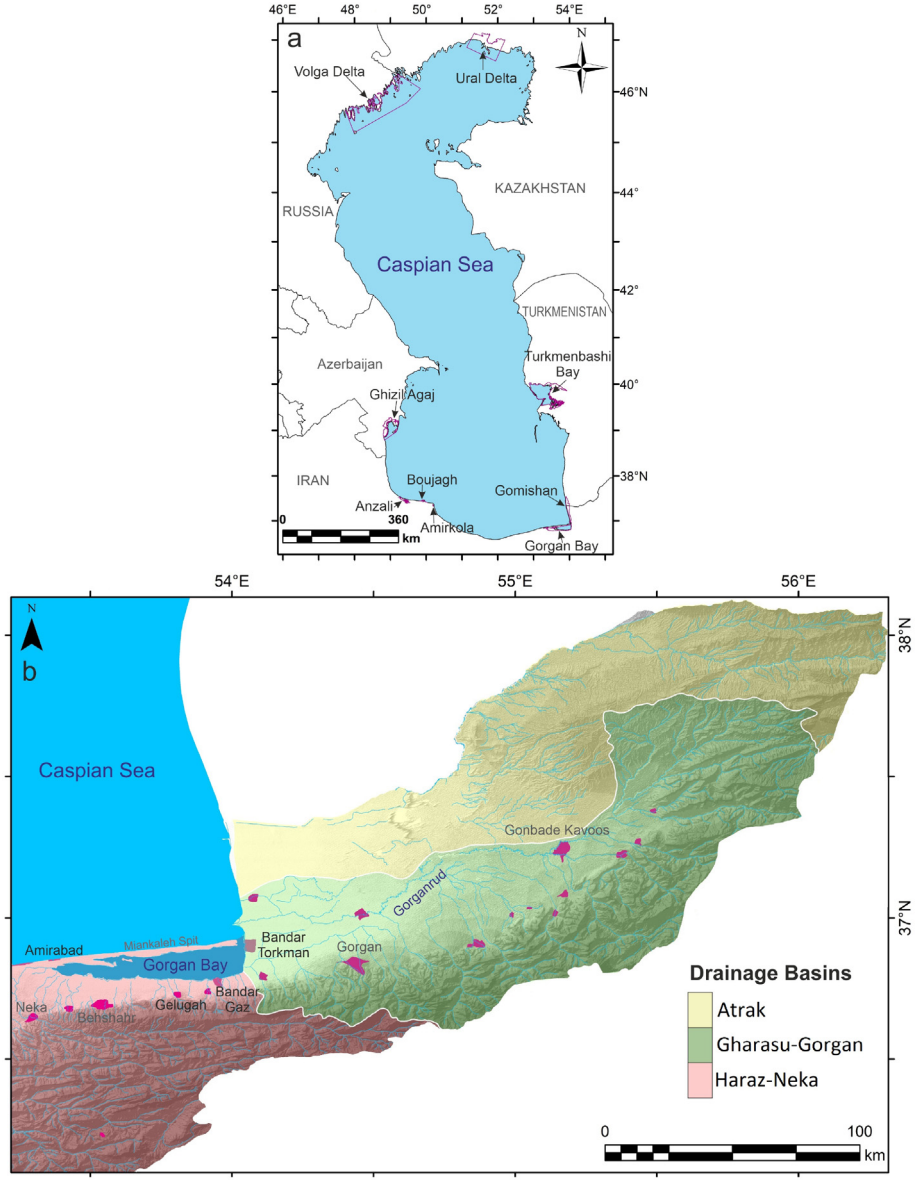

Fig. 1. The study area showing Caspian coastal wetlands registered as Ramsar sites (a), and Gorgan Bay catchment (b).

exceeds 78,000 km^3 (Nikolaeva, 1971). A newly calculated surface area is 331,800 and 428,500 km^2 at the level of −30 and − 27 m, respectively (Arpe et al., 2019).

Based on geological history and bottom morphology, the CS can be divided into three sub-basins. The North Caspian is rather shallow, with a gentle southward bottom slope and a maximum depth of 25 m. The Middle Caspian basin consists of a deep basin with a maximum depth of 788 m in the center, a narrow shelf in the west and a wide shelf in the east. The South Caspian basin with a maximum depth of 1025 m includes the bulk of the water volume and is separated from the middle basin by the Apsheron Sill at a depth of 150 m (Voropaev, 1986).

The coast of the CS with a total length of 7500 km extends over five coastal states (Kosarev, 2005). The general outlines of the Caspian coast largely depend on the geological background of the Caspian basin and adjacent territories. The coast of the northern Caspian with a gentle slope is located in the south of the Russian platform. Extensive river deltas, sand dunes, old sea terraces and river valleys are the main geomorphological features of the northern Caspian coast. The eastern coast of the CS is characterized by the absence of river flow and preponderance of carbonate sedimentation (Leontiev et al., 1977). The catchments of the western and southern coasts are located in the Caucasian and Alborz Mountain belts, respectively. About 130 rivers flow into the CS through the northern, western and southern coasts (Rodionov, 1994). The southern and western coast rivers originate in steep mountains, delivering clastic sediments to the coast, often in a catastrophic way (Leroy et al., 2022b).

The Caspian river mouths, coastal lagoons and beaches are a highly productive environment that provide ecosystem services. The Caspian coastal wetlands are a valuable environment for fish reproductions, bird wintering and breeding. The only large mammal, the Caspian seal, *Pusa caspica*, spends winter breeding on the north Caspian wetland (Goodman and Dmitrieva, 2016). The Caspian coastal wetlands that are enlisted in the Ramsar Convention have a total area of around 14,200 km^2 that mainly encompasses shallow waters as well as adjacent beaches (Table S1, Fig. 1). The two north Caspian Ramsar sites include part of the Volga and Ural deltas and adjacent coasts that are located in a very gently sloping area. Many of south Caspian coastal lagoons and bays have been formed in the last millennia, since the mid-Holocene with the rising CSL, called the Neocaspian transgression (Leontiev et al., 1977; Rychagov, 1997). The development of bar and spits engulfes part of the shallow sea waters and shapes Ghizil-Agaj Bay on the southwest coast, Turkmenbashy Bay on the

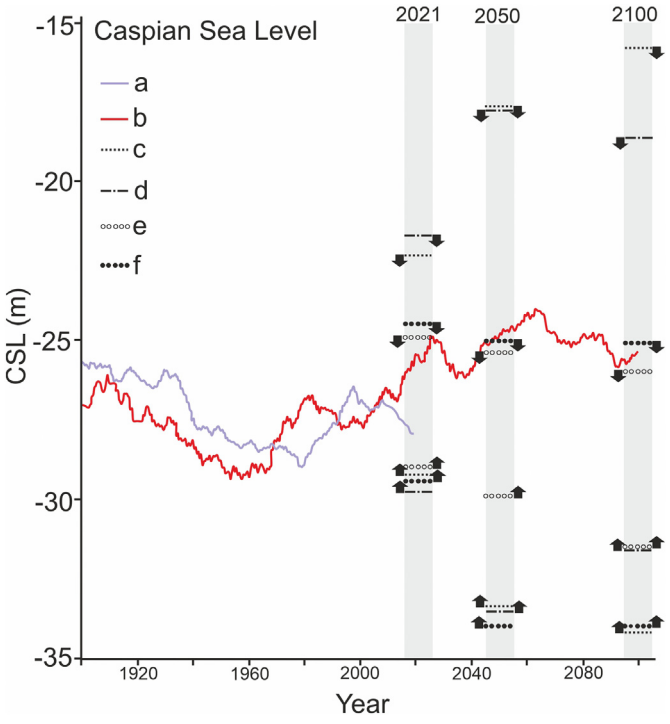

Fig. 2. CSL variability from 1900 to 2100, a) observed, b) reconstructed after Arpe and Leroy (2007), lowest and highest ranges for the forecast of the CSL using different models and four scenarios of shared socioeconomic pathways (SSPs) and representative concentration pathways (RCPs); c) RCP4.5, d) RCP 8.5, e) SSP245 and f) SSP585 for 2021, 2050 and 2100 after Koriche et al. (2021).

southeast coast, Anzali Lagoon and GB on the south coast. Four other south Caspian Ramsar sites (Bujagh National Park, Amirkelayeh Lake (Amirkola), Fereydoon Kenar, Ezbaran & Sorkh Ruds Ab-Bandans, Gomishan Lagoon) have the same origin with younger ages, some formed only at the end of the 19th century (Kakroodi et al., 2012; Naderi Beni et al., 2013; Haghani and Leroy, 2016; Haghani and Leroy, 2020).

2.2. Caspian Sea level

The CS has experienced different sea levels since its isolation from the adjacent seas millions of years ago. Its level oscillated around 90 m in the Holocene, 10 m in the historical period and 3 m during the instrumental measurement period (Varushenko et al., 1987; Forte and Cowgill, 2013; Rychagov, 1997; Naderi Beni et al., 2013). The last CSL rise has happened since 1978 and lasted until 1995. After that, it fluctuated with minor changes that show a generally falling trend, with a sharp one in 2010 (Lahijani et al., 2010; Arpe et al., 2012). The mean CSL during instrumental measurements is −28 m below world sea level (Kosarev, 2005), deviation around 1.5 m or more above that level attributed to high stand and 1.5 m or lower than that level to low stand. When looking at a map and knowing that with the prevailing westerlies the Atlantic is the main moisture source for Europe, one would consider that the main source for the variability of the CSL is from atmospheric circulation variability due to the north Atlantic oscillations (NAO), a link investigated by many scientists (e.g., Nandini-Weiss et al., 2019). However already in 2000, Arpe et al. recognized that the variability of the CSL can be simulated by integrating *El Niño–Southern Oscillations* (*ENSO*) anomalies in time and concluded that ENSO is most likely the main atmospheric driver for the CSL variability. During El Niño events, the subtropical jet stream moves further to the south (Arpe et al., 2020) and, with it, the baroclinicity and cyclone tracks which are accompanied by increased precipitation over the CS catchment area. A jet stream shift similar to that of the ENSO was found by Nandini-Weiss et al. (2019) with strong NAO events.

The current sea level (2022) is around 1.91 m lower than that in 1995 (Fig. 2). Riverine water influx into and evaporation over the CS are the two main water balance components whose relative changes determine sea level. Arpe et al. (2013) demonstrated the possibility to simulate the CSL variability by calculating the water budget from ECMWF re-analyses data (Dee et al., 2011; ECMWF_ERAinterim, 2018). Direct water consumption in the catchment basin accounts for one meter decline in the sea level since the 1960s, after major dam constructions, which acted both during sea level fall and rise (Frolov, 2003). Atmospheric climate forcing contributes to moisture transfer and evaporation regime over the CS and catchment basin that is responsible for sea level rise and fall. Long-term climate prediction indicates a higher temperature for the CS and catchment

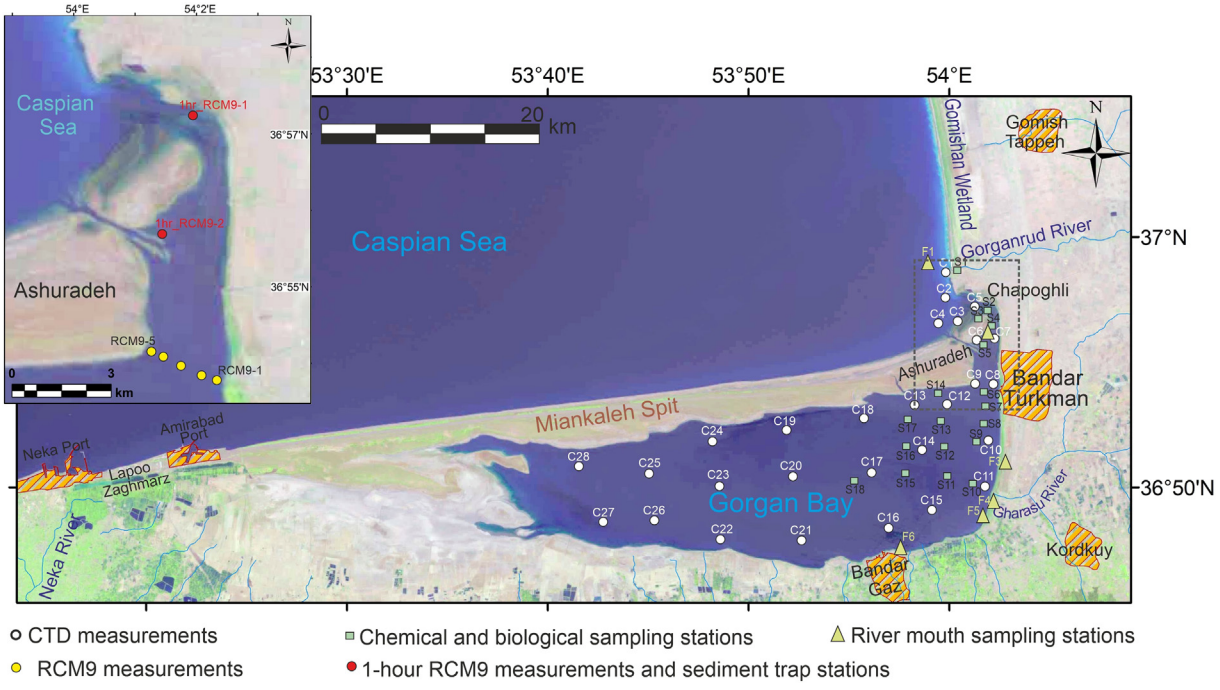

Fig. 3. Location of the stations for the measurement and sampling network in the Gorgan Bay.

and variable precipitation (IPCC, 2013). A decrease in precipitation will occur in the southern part of the CS catchment; however, higher latitudes will benefit from excess precipitation. This could stabilize the CSL in the current falling trend or one would expect further decline in case of higher water consumption. With increasing CS temperature, which is expected in the 21st century due to global warming, an increase of evaporation over the CS is likely. From this Chen et al. (2017) deducted that the CSL should fall in the 21st century. That need not happen as most of the increased evaporation will fall as precipitation within the CS catchment area. Arpe et al. (2020) found that a fall of the CSL with enhanced evaporation will only happen when there would also be enough westerly winds, which would blow the humidified air to the east and lead there to an increase in water levels in central Asian lakes. Arpe and Leroy (2007) used climate simulations to test the ability of the model simulation, the simulations started with pre-industrial time with climate forcing (CO_2, aerosol, solar parameters and others) as known until 2000 and then used estimated climate forcing after that (Fig. 2) and found that with their model and prescribed climate forcings, the simulations were able to reproduce the observed CSL variation until 2000 and got an increase of the CSL for the 21st century. More recent simulations were investigated by Koriche et al. (2021) who showed a wide variation in the CSL change for the 21st century, mostly with a decline of the CSL, partly distinguished by the prescribed CS size: increases when the models used larger CS sizes and declines with smaller CS sizes (Fig. 2). We have to conclude that the future of the CSL is not known yet.

2.3. Gorgan Bay

The GB on the southeast coast of the CS in Iran is 60 km long and 12 km wide with a maximum depth of around 3 m. Miankaleh Spit nearly cuts off the GB from the CS (Fig. 1b). The formation of the GB is attributed to the enlargement of the Miankaleh Spit due to a strong eastward longshore current since the mid-Holocene CSL high stand (Lahijani et al., 2009; Kakroodi et al., 2012). Several shore-parallel sandy-gravelly islands have merged and then allowed the separation of the GB from the CS. The CSL fall and sedimentation detached the westernmost part of the GB and transformed it into isolated shore parallel lagoons called Lapoo and Zaghmarz. Further west the old extension of the GB is buried by alluvial deposits and soils (Lahijani et al., 2009). The current lagoons and spit (Miankaleh Peninsula, GB & Lapoo-Zaghmarz Ab-bandan, coordinates: 36°49′39″N 53°41′49″E) were designated as Ramsar sites in 1979 and the spit was designated as Biosphere Reserve in UNESCO in 1976 (UNESCO, 2022).

The GB catchment area is one of the CS sub-basins which is located in Golestan and Mazandaran coastal provinces with a small part located in the Kopet Mountains or Kopet-Daq (north Khorasan province) (Fig. 1b). The area of the GB watershed located in its southern part is about 3000 km^2 and includes two side rivers that affect the GB during flooding (Gorgan River, or Gorganrud, 12,600 and Neka River 3000 km^2) and is about 18,600 km^2, most of which are mountainous areas and the rest are foothills and plains. A few ephemeral rivers enter the GB, the only permanent river is the Gharasu that brings annually around 54 million km^3 of water into the GB. The Gorganrud River flows into the CS in the proximity of the GB main inlet (Fig. 1b, Fig. 3). During extreme flooding, part of the Gorganrud water diverts into the GB. The GB water is brackish, and its salinity is around 13–18 Practical Salinity Scale, which is higher than the adjacent Caspian waters at 11.8 Practical Salinity Scale measured in Feb. 2014 (Leroy et al., 2018).

The climate on the south Caspian coast is subtropical where precipitation significantly decreases from west to east. The GB and its catchment basin are located on the easternmost of the southern shoreline. The overall climate in the west part of the watershed is Mediterranean and in the east part semiarid. The imprint of the climate is visible in the catchment basin which is covered by vegetation in the west part and has a baren landscape in the east. The annual precipitation, mean temperature, and De Martonne indices for different stations at the GB are shown in Table 1. The highest precipitation falls in the west of the GB and the lowest in the easternmost area (Bandar Turkman, or Turkmen Port). Evaporation is the most important factor that causes the loss of the bay water. The highest annual evaporation rate is related to the Turkmen port at 1552 mm. The station also has a higher average temperature than the western parts of the GB (Table 1, Fig. S1). Annual average of daily maximal and minimal temperature are 22 °C and 14 °C, respectively. The lowest recorded temperature in the GB coastal area occurred in winter in 2021 (−9 °C) and 2015 (−5.5 °C). The highest recorded summer temperature is also in 2021 (40.8 °C) and 2015 (42.1 °C).

Table 1
The climate of the Gorgan Bay area.

Station	Annual precipitation	Mean temperature	De Martonne Index	Climate
Turkman	466.95	18.21	16.55	Semiarid
Gaz	537.5	18.4	18.92	Semiarid
Galugah	588.9	17.64	23	Mediterranean
Amirabad	636	17.65	21.3	Mediterranean

Wind and wave climate at the seaside of the Miankaleh Spit are dominated by a northwest direction (Terziev et al., 1996).

3. Materials and methods

In this study, we have used five kinds of datasets that include satellite images, measured hydrometeorological data, reanalysis meteorological data, measured parameters in the GB, and finally retrieved data from sampling in the GB that underwent laboratory analysis. The satellite images have been used for mapping the circum-Caspian Ramsar sites. We gathered measured hydrometeorological data for analysis of the climate around the GB as well as the CSL changes. We used reanalysis data as input data for dust simulation. With measured physical parameters in this study in the GB, we calibrated and verified the simulation of the water circulation. Laboratory-analysed data were used to assess water quality of the GB and rate of sedimentation in the main inlet. We applied the datasets for assessing past changes in the wetlands, evaluating the current condition of the GB and forecasting its future condition. Different aspects of the sampling and measurement data as well as data analysis and simulation are elaborated in the following sub-sections.

3.1. Satellite images and hydrometeorological data acquisition

In this study, Landsat satellite images of 1978, 2021 (two low stands) and 1995 (high stand) downloaded from a USGS website (https://earthexplorer.usgs.gov) were used to determine and calculate the coastline and the area of the lagoons and the bays. All Landsat images are attributed to June and July to eliminate a possible influence of seasonal variation in water level. We excluded the Fereydoon Kenar, Ezbaran & SorkhRuds Ab-Bandans wetland on the south coast because they did not have connections with the Caspian Sea during the study periods. Our focus was on the changing in area due to the sea level rise and fall, therefore the total wetland area even in the extreme high stand of 1995 is less than the registered area in the Ramsar sites. The reason for this difference is that the registered area includes adjacent beaches, spits and islands that, by definition, are wetlands, but are beyond the sea level of 1995.

Data from four weather stations of the Iranian Meteorological Organization (IRIMO) were selected to analyse the parameters of precipitation (mm), air temperature (°C) and evaporation (mm) (Table S2, Fig. 1b). The Amirabad and Ashuradeh as well as the Caspian rim stations for sea level available at CASPCOM (http://www.caspcom.com) were also used.

3.2. Field campaigns

The main goals of the field campaign were as follows: to know the existing water quality, to estimate sedimentation rate in the main inlet, to assess water exchange between the GB and the CS and to use data of the

water currents for water circulation simulation. One of the main issues for the field campaign in the shallow depth of the GB inlet was concerning the installation of current meters and sediment traps. In the first attempt, we lost sediment traps that were fortunately not costly. For the following time, we installed current meters and sediment traps simultaneously and hired surveillance to be sure to retrieve our valuable instruments and data.

Field campaigns were conducted in the GB in 2020 (Fig. 3). In-situ measurements of water column properties including temperature, conductivity, pressure, dissolved oxygen and pH were obtained using a CTD 75 M, Sea & Sun Technology probe. The CTD was calibrated before application to each field measurement. Water samples for determining dissolved nutrients were filtered by syringe filter (0.45 μm cellulose acetate) and collected in high-density polyethylene bottles and frozen till analysis (Grasshoff and Ehrhardt, 1999). Water sampling was repeated for nutrient analysis and phytoplankton collection, the former fixed with formalin 5 % and the latter using lugol. For zooplankton sampling, we pulled a 100 μm mesh net with a circular opening (diameter of 50 cm) which included a water collector. We sampled 500 ml of the water containing zooplankton and fixed it with 4 % formalin.

Five RCM9 current meters were installed in the main inlet of the GB for 15 days (1–15 August 2020) with 20 min time intervals and short-term measurements conducted in two inlets (Ashuradeh and Chapoghli) (Fig. 3, Table S3). Current speed and direction as well as pressure (depth) and temperature were measured by the current meters. Adjacent to the current meters, four sediment traps were installed for load deposition for the same period of time (Fig. 3). In order to determine the sedimentation rate in the GB, four sediment traps were used in the water column (near the bed). Each sediment trap consists of cylindrical PVC pipes with a length of 30 cm and an opening diameter of 10 cm. For preventing trash being trapped inside the trap, the open end of the sediment trap was covered with nets with a mesh size of 10 mm. Sediment traps were fixed on near the RCM9 and close to the inlet bed in the water column. After two weeks, the sedimentation traps were recovered and transferred to the laboratory to determine the sedimentation rate. This type of sedimentation trap was selected based on previous works done in aquatic environments (White, 1990; Kozerski, 1994; Szmytkiewicz and Zalewska, 2013).

3.3. Laboratory analyses

3.3.1. Nutrient analysis

Measurement of nutrients (phosphate, nitrate, nitrite and ammonium) was obtained by colorimetric method using an ultraviolet-visible spectrometer, Analytik Jena, specord 210. Ammonia was determined by the hypophenol oxidation blue dye method (Koroleff, 1983). Nitrate and nitrite were analysed using the reduction column and pink azo dye method (Wood et al., 1967). Phosphate analysis was based on the formation of the phosphomolybdate complex (Murphy and Riley, 1962).

3.3.2. Plankton counting

For phytoplankton identification, water samples taken from each station were kept in a cool dark place for one week to completely precipitate the plankton. After that, the surface water was siphoned and drained until the remaining water volume reached 50 cc. The samples were then centrifuged using a centrifuge at 3000 rpm for 5 min. The supernatant was siphoned and drained again, and the remaining water volume was reduced to 25 cc. After this step, 1 ml of the remaining water containing phytoplankton samples was poured on the SEDGEWICK-RAFTER slide. The phytoplankton was identified and counted using an optical microscope and reliable keys. For zooplankton, we used the Bogorov slide and invert microscope for identification and counting.

3.3.3. Sedimentation rate

The samples for sedimentation rate were dried at 105 °C and weighted. They were burnt at 550 °C in a furnace for measuring organic materials (Heiri et al., 2001). The sedimentation rate was estimated following the method of Szmytkiewicz and Zalewska (2013).

3.4. Atmospheric and marine simulations

3.4.1. Dust simulation

Dust emission is a current challenge in this region at the transition from Mediterranean to semi-arid and arid climate. The adjacent Ramsar site, the Gomishan Lagoon (Figs. 1 and 3), based on our observation in 2020 almost desiccated totally. This is a warning for future threats to the GB. The dust simulation was applied to the GB to assess whether the GB will become a dust source in case of desiccation and how its desiccation would impact the surrounding areas.

In this research, the Weather Research and Forecasting model coupled with Chemistry (WRF-Chem) model version 3.9.1 (Skamarock et al., 2019) were used to simulate the effect of the GB drying on dust emission in the region. WRF-Chem is a chemistry version of WRF that simulates the emission, transport, mixing and motion of airborne particles (Grell et al., 2005). In general, there are 33 options for selecting land vegetation in the WRF model. In this research, the input model data was modified, so that the GB area was considered as a dry area with little vegetation. Soil material was considered as a proportion of sand and clay, which is about 80 % sand and 20 % clay and vegetation cover was selected as low grass. The first 12 h of the run were considered as spin-up. Also, a Hybrid Single Particle Lagrangian Integrated Trajectory (HYSPLIT) model was used to generate an ensemble of forward trajectories to trace the trajectory of the dust particles in the GB area (Stein et al., 2015; Rolph et al., 2017).

3.4.2. Water circulation

We employed simulation of water circulation in the GB to assess how the GB water interacts with the CS waters trough inlets. It helped evaluating the GB water residence time and its rate of renewal that determines water quality. The result of this simulation will guide us to see if the inlet maintenance will be a proper decision for the GB restoration.

The FVCOM hydrodynamic model was used in the GB, which is a general volume water circulation model with a finite volume method. This model is very suitable for estuaries, shallow seas with complex topography, as well as for seas with complex islands and beaches. This model uses a flexible triangular grid that allows the distance between nodes to be changed. FVCOM has a prognostic, unstructured-grid, finite-volume, free-surface, three-dimensional (3-D) primitive equation developed originally by Chen et al. (2003). This model discretizes and solves equations using the integral method. In this method, mass stability is guaranteed. Technically, this method is similar to the finite difference method in terms of simplicity in coding and similar to the finite element method in terms of flexibility in the shape of beaches and land structure. The governing equations that are solved by the model using the finite volume method include the equations of momentum, continuity, temperature, salinity, density, and equation of state (Chen et al., 2006). The model ran in cold start mode for the year 2019 and was calibrated and verified with measured data (current meter and CTD data). Input data consisted of sea level fluctuations, temperature and salinity time series at the open boundary and atmospheric forces (wind, evaporation, precipitation and heat fluxes data) at the domain. The domain forces were constant in space and variable in time. Finally, the stabilized model ran for low stand and high stand scenarios with the prevailing conditions of its time. Model forces for the different times were used from ECMWF atmospheric data (https://www.ecmwf.int/en/forecasts/datasets). Open boundaries data were generated from the Copernicus site (https://marine.copernicus.eu/).

We calculated flushing time in the current condition and in future scenarios with enhanced water exchange between CS and GB. The minimum flushing time T_f is the volume of the GB divided by the volume of incoming water. A decrease in flushing time leads to an increase in

water quality. A simple relation for calculating flushing time is written in Eq. (1).

$$T_f = \frac{V}{Q_b} \quad (1)$$

where

$$Q_b = Q_s + Q_r \quad (2)$$

where T_f is water flushing time in the GB, V is total GB volume, Q_b is total volume of rivers (Q_r) and CS (Q_s) and considering of V at 0.6 km^3 area about 450 km^2 and average depth of 1.5 m.

4. Results

4.1. Caspian Ramsar sites during the past half-century

The general trend of the CSL fall in 1960s and 1970s caused shrinking of the Caspian Ramsar sites where their total area reached 9810 km^2 in the extreme sea level fall of 1970s (Fig. 4). During subsequent sea level rise, they regained the area and in the extreme rise of 1995 the total area reached 13,413 km^2. All the wetlands and bays show an increase in area in the 1995 high stand phase, except Amirkola that shows 9 % reduction in surface area. In the south coast, the Gomishan Lagoon, by far, has experienced the most expansion and in the north coast, the Ural Delta. A minimal area

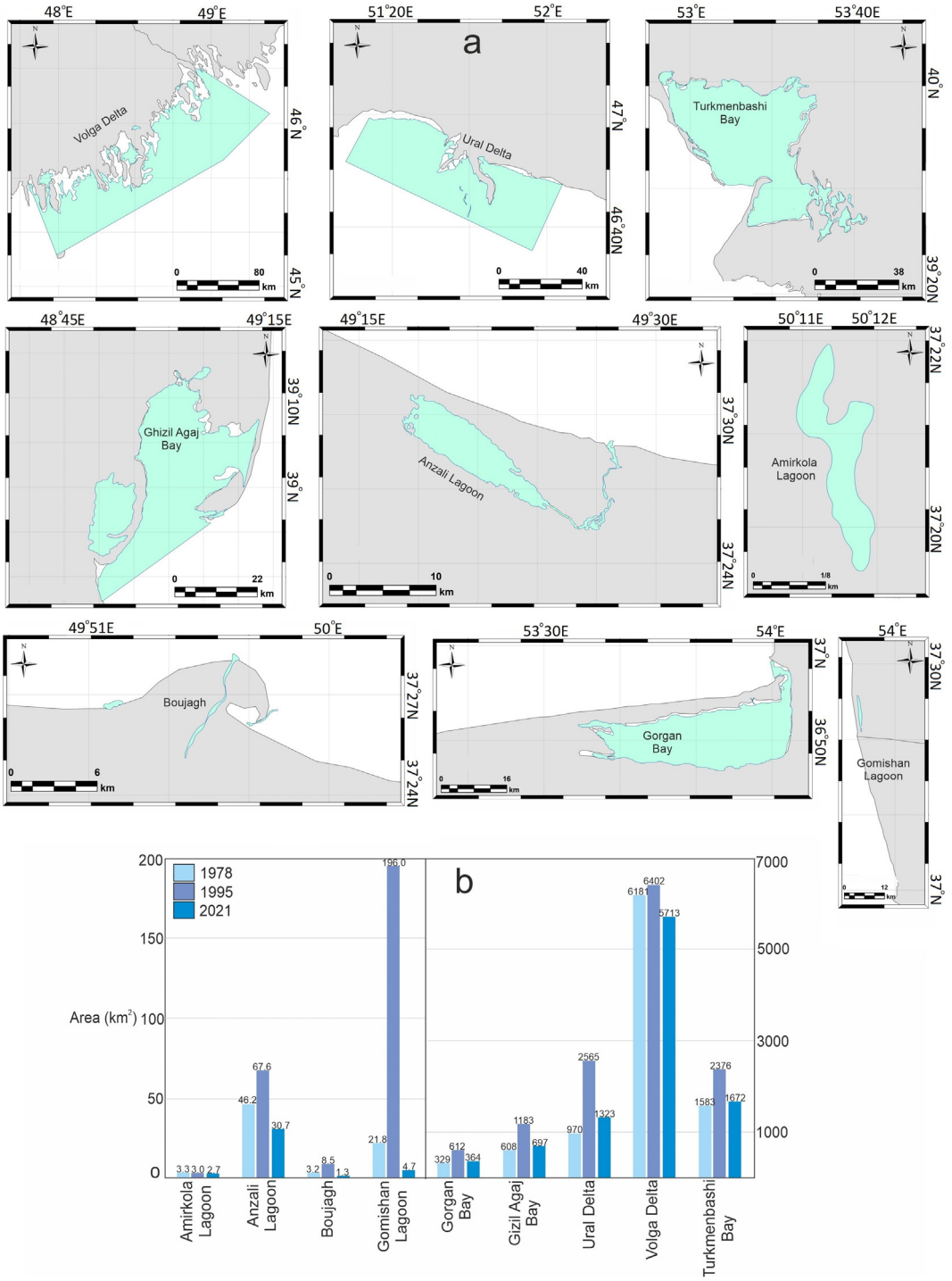

Fig. 4. The surface area of the Caspian coastal wetlands that were registered in the Ramsar sites, in 2021. a) and wetlands area in 1978, 1995 and 2021 in b).

expansion from 1978 to 1995 was observed in Volga wetland with around 3.5 % only. Since 1996, sea level dropped around 1.9 m and the total area of the wetlands was reduced to 9745 km^2 (Fig. 4a&b). The Gomishan Lagoon in the current sea level fall has also experienced the highest shrinkage, which has almost desiccated compared to the high stand of 1995 and the low stand of 1978. The decrease in area from 1995 to 2021 is also obvious in Bujagh, Anzali, Amirkola and Volga with a 85, 55, 10 and 11 % decrease respectively. On the other hand, the present area of Ural, Gizil-Agaj, GB and Turkmenbashi is 27, 13, 10 and 6 % larger than that of the 1978 low stand period. However, other south Caspian wetlands have shrunk more in the current sea level fall, which is still around 60 cm higher than that of 1978 (Fig. 4, Fig. S2).

4.2. The Gorgan Bay

4.2.1. Biological component

Based on the results of this study, in the sampling stations of GB, a total of thirteen phytoplankton species from five phyla were identified. The Bacillariophyta had the highest number of species. The lowest number of species belonged to Euglenophyta and Chlorophyta (Fig. 5). By comparing the number of species in the two studied seasons, the highest number of phytoplankton species was observed in spring (May 2020) and the lowest number in summer (August 2020).

The percentage of species abundance of the identified phytoplankton varies in different phyla. Accordingly, in spring, Bacillariophyta had the highest percentage of species abundance (38 %) and Chlorophyta had the lowest percentage of species abundance (8 %) of the total identified species. In summer, Pyrrophyta had the highest percentage of species abundance (40 %). Euglenophyta also had the lowest percentage of species abundance (10 %) of all identified species.

In the spring, *Prorocentrum micans* had the highest abundance (14.3 million individuals per m^3) in all studied stations. Also, the lowest abundance of phytoplankton in all studied stations belonged to *Euglena* sp. (100,000 individuals per m ^{3}). In summer, *Exuviaella cordata* was the most abundant (7,700,000 individuals per m ^{3}), while the lowest abundance of phytoplankton in all stations belonged to *Actinocyclus* sp. (400,000 individuals per m ^{3}) (Fig. 5).

The values of the Shannon diversity index of phytoplankton species in each of the studied stations in spring and summer are shown in Table 2. The highest value of the Shannon diversity index in spring was calculated in station 6 (2.185) and the lowest value was calculated in station 4 (2.055). In summer, the highest value of the Shannon diversity index was calculated in station 17 (2.224) and the lowest value was calculated in station 15 (1.780). By comparing the Shannon diversity indices between the two studied seasons, no significant statistical difference was observed in terms of calculated values ($p > 0.05$). According to the values of Shannon diversity indices of phytoplankton species in different stations in two seasons, it seems that in terms of water quality classification, GB has moderate conditions.

Table 2
Values of the Shannon diversity indices for phytoplankton species in two seasons (May and August, 2020).

Station	Spring	Summer
1	2.121	2.125
2	2.172	2.039
3	2.169	2.121
4	2.055	2.020
5	2.115	2.128
6	2.185	2.210
7	2.095	2.122
8	2.165	1.985
9		1.995
10		2.011
11		2.023
12		2.218
13		1.880
14		2.180
15		1.780
16		2.111
17		2.224
18		2.133

Based on the results of this study, two groups of zooplankton were identified in the sampled stations, including (Copepoda) (*Acartia tonsa* and Nauplius of *A. tonsa*) and the larval stages of Nauplius of *Balanus* sp. - Cypris of *Balanus* sp. According to the results in spring, *A. tonsa* had the highest abundance (15,850 individuals per m ^{3}) and Nauplius of *Balanus* sp. larvae had the lowest abundance (180 individuals per m ^{3}). In summer, *A. tonsa* had the highest abundance (9290 individuals per m ^{3}). However, the lowest abundance belonged to Cypris of *Balanus* sp. larvae (40 individuals per m ^{3}). According to the results, *A. tonsa* had the highest frequency in the studied stations in both spring and summer. Also, members of the Copepoda had the highest frequency in all studied stations (Fig. S3).

The values of Shannon diversity indices of zooplankton in each of the studied stations in spring and summer are shown in Table 3. The highest value of the Shannon diversity index in spring was calculated in station 4 (0.6218) and the lowest value was calculated in station 6 (0.5024). In summer, the highest value of the Shannon diversity index was calculated in

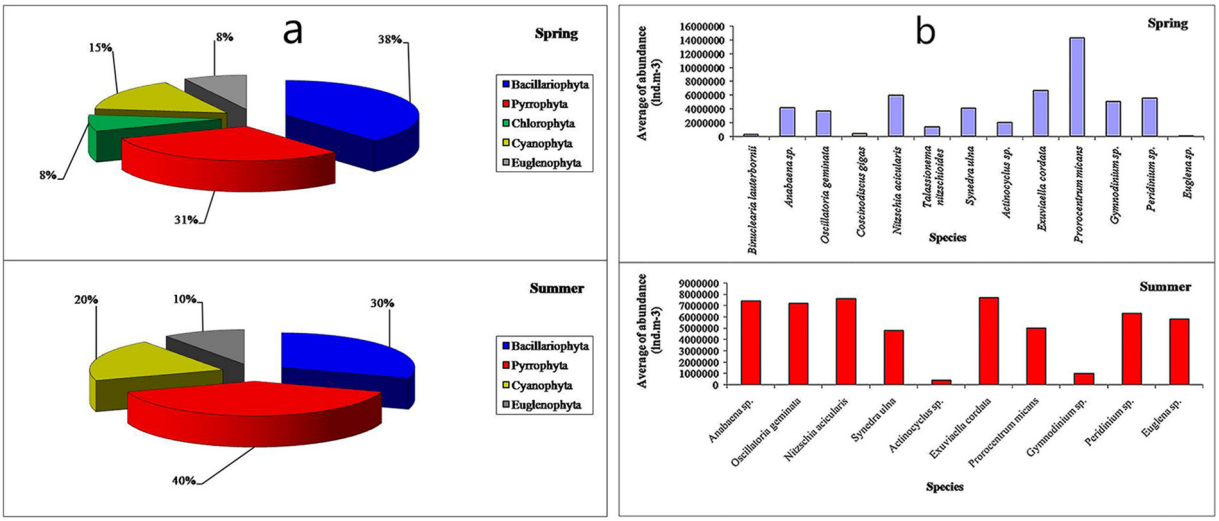

Fig. 5. a) Percentage of species of each of phytoplankton groups identified in spring and summer, b) Overall abundance of each of the phytoplankton species identified at the studied stations.

Table 3
Values of Shannon diversity indices for zooplankton species in two seasons (May and August, 2020).

Station	Spring	Summer
1	0.5911	0.6099
2	0.5238	0.4308
3	0.6111	0.6431
4	0.6218	0.4321
5	0.5684	0.5620
6	0.5024	0.6312
7	0.6087	0.6110
8	0.6136	0.5530
9		0.4465
10		0.6712
11		0.4021
12		0.4110
13		0.6650
14		0.6150
15		0.5820
16		0.6032
17		0.6314
18		0.6558

station 10 (0.6712) and the lowest value was calculated in station 11 (0.4021). By comparing Shannon diversity indices between two studied seasons, a significant difference was observed between some of the stations ($P < 0.05$). According to the values of Shannon diversity indices of zooplankton species in different stations in the two studied seasons, it seems that GB water quality has bad conditions in terms of classification.

4.2.2. Hydrochemistry and nutrient distribution

The average suspended load in May is 30.75 mg / L and the range of changes is 23 to 43 mg / L. The average suspended load in August is 33.22 mg / L and the range is 24 to 48mg / L. In stations 1 and 10, the amount of suspended load is high due to the water inflow of the Gorganrud and Gharasu, respectively (Fig. S4). Nutrients values in the waters of GB in May and August are shown in Tables 4 and 5.

The average phosphate ($PO4^{3-}$) in the surface waters of GB in May was 14.38 μg / L and its changes ranged from 7 to 21 μg / L. In August, the average phosphate was 10.56 μg / L and the range of changes was 5 to 18 μg / L.

The average nitrate in May and August was 1312.131 and 796.56 μg / L, respectively, and its changes in the range of 850 to 1356 μg / L were obtained in May and 321 to 1359 μg / L in August.

The average concentrations of nitrite and ammonium in May were 8 and 112 μg / L, respectively, and in August were 5.26 and 68.11 μg / L,

Table 4
Nutrient concentration ($\mu g.l^{-1}$) in the Gorgan Bay (August 2020).

St.	$P\text{-}PO_4^{3-}$	$N\text{-}NO_2^-$	$N\text{-}NO_3^-$	$N\text{-}NH_4^+$
1	15	6.31	925	91
2	13	5.89	931	84
3	10	8.11	750	65
4	16	5.22	452	76
5	7	4.44	1211	46
6	9	6.13	972	39
7	13	3.22	375	84
8	18	4.51	659	65
9	10	6.22	854	51
10	15	5.26	989	85
11	6	7.22	1359	79
12	11	3.67	798	58
13	12	5.56	875	87
14	7	6.89	523	65
15	9	3.00	321	49
16	5	4.44	746	69
17	8	5.26	542	85
18	6	4.44	1002	48
Mean	10.56	5.26	793.56	68.11
Max	18	8.11	1359	91
Min	5	3.00	321	39

Table 5
Nutrient concentration ($\mu g.l^{-1}$) in the Gorgan Bay (May 2020).

St.	$P\text{-}PO_4^{3-}$	$N\text{-}NO_2^-$	$N\text{-}NO_3^-$	$N\text{-}NH_4^+$
1	17	9	1223	89
2	21	7	950	121
3	15	8	1102	95
4	13	11	998	54
5	16	5	850	102
6	10	8	1356	77
7	7	6	1201	211
8	16	10	1329	151
Mean	14.38	8	1126.13	112.50
Max	21	11	1356	211
Min	7	5	850	54

respectively. The range of concentration changes for nitrite and ammonium in May was 5 to 11 μg / L and 54 to 211 μg / L, respectively.

In August, the range of changes for nitrite is 3 to 8.11 μg / L and for ammonium is 39 to 91 μg / L (Fig. S5).

4.2.3. Inlet sedimentation rate and Miankaleh wave

All sediment traps show high sedimentation rates, ranging from 1.02 to 1.71 cm y^{-1} with an average of 1.43 cm y^{-1}. Organic material content is comprised between 12.3 % and 17.6 % with an average content of 14.9 %.

Measured wave data from the depth of 10 m in the west part of the Miankaleh indicate that the incoming wave has a maximum height of 1.8 m and a period of 8.8 s (Fig. S6).

4.2.4. CTD data analysis

The time series of water temperature and electrical conductivity measured at the location of the current meters are shown in Supplementary fig. 7. The trend of temperature changes is the same for all stations and here only the temperature of one of the measuring stations is shown. Daily changes in temperature during the deployment period were about $1^{\circ}C$. In the deployment period (~ 15 days), water temperature changes were about $4^{\circ}C$.

Fig. 6 shows the depth-averaged of various measurement parameters using a CTD instrument. The maximal and minimal measuring depths of 3.00 and 0.2 m were recorded at the positions of stations 19 and 3, respectively. Fig. 6a shows the horizontal distribution of water temperature at measuring stations. From west to east of the GB, water temperature shows a decreasing trend. The maximum temperature was observed in station 27 with a value of $29.42^{\circ}C$. Also, the lowest temperature was observed at the entrance of GB at about $25.48^{\circ}C$ and at station 3 and at the mouth of the entrance of Ashuradeh Channel.

The horizontal distribution of water salinity (Fig. 6b), as well as the density of water, is similar to the horizontal distribution of water temperature. The maximal amount of salinity and density were observed in the western part of the GB with of 20.26 (10.33 kg/m^3). These values are similar to those measured at water station 27. The lowest salinity and density are observed at the entrance to the GB.

Fig. 6c shows the horizontal distribution of dissolved oxygen at CTD measuring stations. The horizontal distribution of dissolved oxygen was in contrast with the horizontal temperature distribution. In general, with increasing water temperature, the amount of dissolved oxygen decreases, but Fig. 6c shows the opposite trend. The maximal amount of dissolved oxygen was 11.17 ppm and was recorded at station 21. Low amounts of dissolved oxygen were recorded at the entrance of the GB at about 5.16 ppm at station 3.

Fig. 6d shows the distribution of pH. The range of pH changes was between 8.21 and 8.98 and the maximum amount of pH was observed in station 27 with a value of 8.98 units. The values measured at station 27 indicate abnormalities.

4.2.5. Inlet water current

Fig. 7 and supplementary fig. 8 show the current velocity for the five current meters. The maximal value of recorded velocity is 16.72 $cms^{-1}$for the current meter No 1, which is close to the Turkmen port. The highest

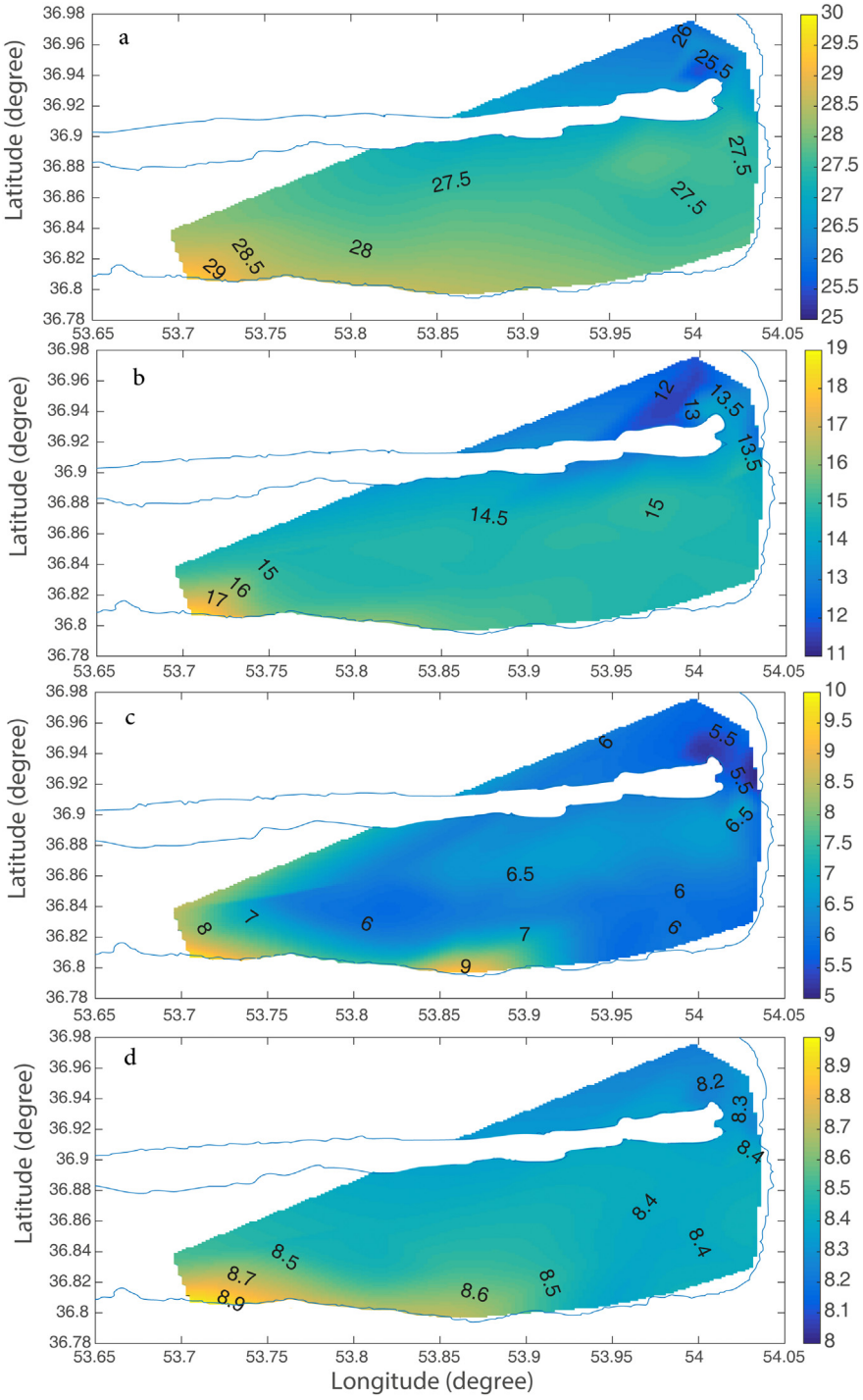

Fig. 6. Depth averaged water properties obtained by the CTD in the GB, a) water temperature (°C), b) salinity (Practical Salinity Scale), c) dissolved oxygen (ppm) and d) pH.

installation depth was related to current meter 4 and this current meter was installed near the inlet bed, the recorded speed values here are somewhat lower compared to other current meters. All current meters from 18:00 to 19:00 on the third of August recorded a significant current speed with northward direction (about 12°, Fig. S8). The second maximum recorded current for all current meters occurred with a slight difference at noon on 12 August. During this period, a high value of current is also recorded. The direction of flow in this period is recorded at about 200 degrees (approximately southwest). The average wind speed based on the nearest meteorological station (Bandar Turkman) during the two high current velocity periods was 7 ms^{-1} with maximum of 13 ms^{-1}.

The average velocity measured at the five stations is estimated to be about 2.5 cms^{-1}. The maximum value of the average velocity was measured at the third station (current meter located in the middle of the channel) and recorded with a value of 3 cms^{-1}.

A major water exchange is in the measured range in the north-south direction (Fig. S8). This major share of currents measured in this period indicates that the water exchange was more from the CS to the GB, although in some cases from the measurement period the direction of flow from the GB to the CS. The measured velocities fall mainly in a range that are <5 cms^{-1} and for velocities <5 cms^{-1} the share of currents about 2 cms^{-1} is higher than the rest.

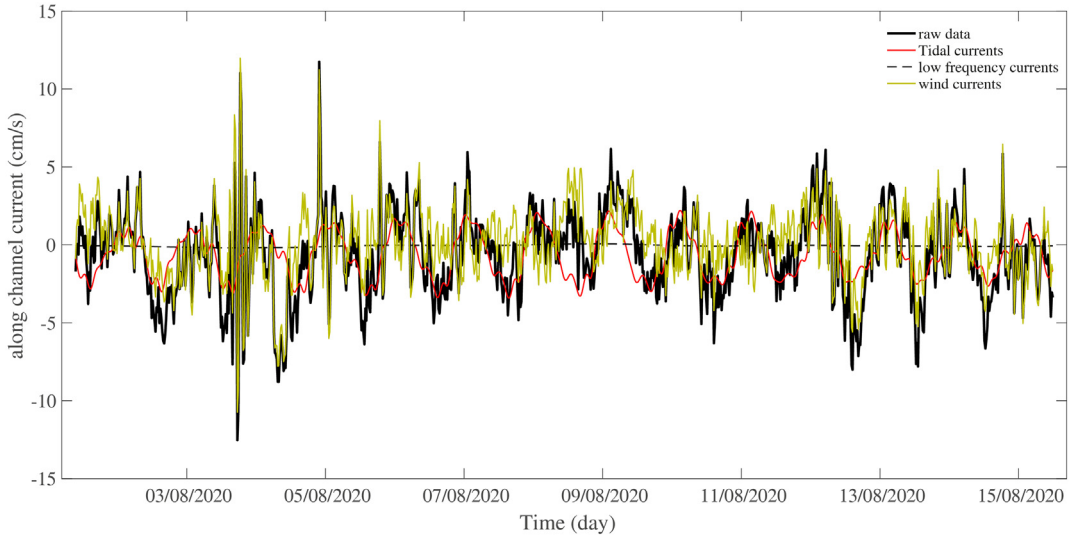

Fig. 7. Share of different currents from field measurements between Turkmen and Ashuradeh main inlet), negative values denote currents into the GB and positive out of GB into the CS. Low frequency currents have very low velocity that seem close to zero.

The share of different currents including wind driven, tidal currents and low-frequency currents (more than ten days) has been calculated and specified (Fig. S9). The share of tidal currents is measured using the u_tide method (Codiga, 2011), the share of low-frequency currents is measured using the Lanczos method (Emery and Thomson, 2004) and the share of wind currents is calculated using the difference between the sum of tidal and low frequencies currents from the total measured currents. The main currents in this area are thus wind currents. The share of the tidal current is also significant relative to the general current. The contribution of low-frequency currents (due to density difference) is very small (Fig. 7).

To compare the current velocity in spring and summer (peak growth of aquatic plants at the entrance of GB in spring and the time of decline of these plants in summer) current meters were installed for about an hour in the two mentioned seasons at the narrow entrance channel (Chapgholi Channel). A comparison of measurement results shows that the velocity of the current in summer is higher than in spring. The maximum velocities for spring and summer are 22.88 and 39.89 cms^{-1}, respectively. The average velocities for these two seasons are 12.77 cms^{-1} and 32.00 cms^{-1}, respectively. Other parameters should be considered, including weather conditions, but the decline and destruction of existing seagrass have an important role in water exchange between the CS and GB. A current meter was also installed in the narrow Ashuradeh Channel for 1 h. The maximum speed in this channel is about 29.62 cms^{-1} and the average flow rate in 1 h is about 25.5cms^{-1}.

4.2.6. Dust simulation

The WRF-Chem model was run for 4-days and in different seasons of the year to take account weather conditions in the region during the whole year. The dates were selected in such a way that no precipitation would have occurred in the study area in the previous week; so that soil moisture is low and dust particles could rise from the ground. On 14 February 2016, if the GB is dry, a source of dust would be created. In the next 48h, this source of dust also would be available, which would be weakened and strengthened in some hours. On 5 March 2018, the concentration of dust generated is high and its expansion due to atmospheric currents and south winds to the north is the source of dust. By weakening the southern wind, the transfer of dust to the north is reduced. In the following 48 h, due to the weakening of the wind speed, the intensity of the dust decreases. On 12 July 2019, a slight dust arises from the dust source, but after 24 h, due to the increase in wind speed, the dust concentration increases (Fig. S10).

The time series of dust concentration (μgkg^{-1}-dry air; green line) and wind speed (ms^{-1}; black line), in two sections of Bandar Gaz and Bandar Turkman port for three selected cases. In almost all cases, the maximal and minimal wind speeds correspond to the maximal and minimal dust concentrations. In fact, as the wind speed increases, more dust rises from the dust source and is injected into the atmosphere. The highest dust concentration is related to 5 March 2018, when the dust concentration reaches about 3500 (μgkg^{-1}-dry air). At this time, the wind speed is 8 ms^{-1}, which is a high amount (Fig. S11). The HYSPLIT model provides result for a forward 24 h trajectory with 27-member meteorological ensemble at synoptic weather stations in the near GB at 100 m above ground for different selected cases.

On 14 February 2016, for up to 24 h, dust particles may spread to the west and north of the GB. But there is not much convergence and there is uncertainty. On 5 March 2018, there is more convergence and less uncertainty in the results and there is a possibility of dust particles spreading to the northeast of the GB. On 12 July 2019, there is a possibility of dust particles spreading to the west and south of the study area, although there is uncertainty and divergence in the results (Fig. S12). Dust emission in the GB region would be highest when the pressure gradient between high-pressure and low-pressure is considerable over the region. Moreover, dust could be transported 60 km away from the source and vertically up to 2500 m above the ground.

4.2.7. Simulation of water circulation

Water current simulation is done with the FVCOM model for several scenarios. The study area and the bathymetry are shown in Fig. 8a. An unstructured mesh for numerical modelling was generated with the SMS software. Simulations of water circulation in the GB were made for the sea level low stand (1977), sea level high stand (1995), current conditions with limited inlets (2020) and with improved inlets.

In the simulation of the 1977 condition, the current in GB is strongly influenced by wind (Fig. 8b). The general circulation of water inside the bay is counter-clockwise in the cold season and clockwise in the warm season and the current near the coast is strongly influenced by wind. The average current velocity in the area between Ashuradeh and Bandar Turkman (main entrance) is about 2 cms^{-1}.

In the simulation of the 1995 condition (Fig. 8c), the current in GB is accelerated and water exchange between the GB and the CS occurs from the main inlet that has expanded and deepened by the sea level rise as well as from a newly connected inlet (Khozeini Channel). The overall pattern of water circulation is similar to those in the condition of sea level fall; however, the velocity of water exchange increases up to 7 cms^{-1} in the high stand condition.

The simulation of the water circulation in the current condition with a water level in a range between of that in 1977 and 1995 but with an inlet with dense seagrasses shows that the overall pattern is the same with the

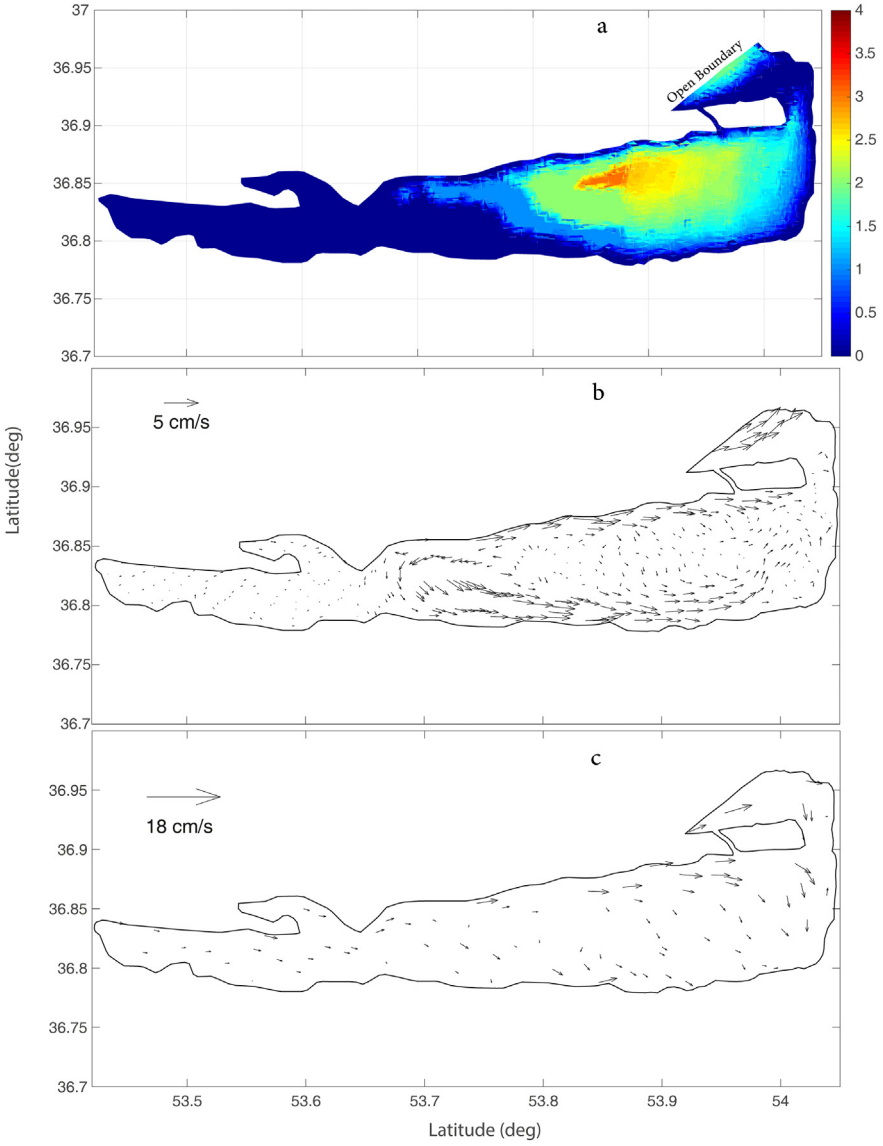

Fig. 8. a) Map of the GB and selected area for numerical modelling with bathymetry, b) Simulated water current for August 1977 (low stand condition), c) Simulated water current for August 1995 (high stand condition).

average velocity exchange of 2.7 cms^{-1}in the main entrance. By removing vegetation (that partially occurs in August after the peak growth in May), the simulation demonstrates an increased velocity in the main entrance in the order of 0.5 cms^{-1}. Dredging of the main channel (with its two inlets) down to 2 m depth and on a width of 200 m will accelerate water exchange with a mean velocity of 3.6 cms^{-1} (not shown here).

For the GB, the main source of inflowing water is supplied from the CS. A stable connection between the GB and the CS requires removal of sediments that accumulated in the GB inlets (Fig. 9c, lower panel). By widening and dredging of the inlets, water exchange between the GB and the CS will significantly be enhanced. An increase in water exchange reduces the flushing time. Calculation of flushing time for field measurement data and model results show that an increase in water velocity from 2.5 to 5 cms^{-1}leads to a decrease in flushing time from 175 to 105 days.

5. Interpretation

5.1. The Ramsar sites

Two Ramsar sites, the Volga and Ural deltas, that are located on the very gently sloping coast of the north CS, have different responses to the CSL fall. The Volga Delta compared to other Caspian coastal wetlands was less affected by the last CSL rise and fall (Mikhailov et al., 2014). The large amount of Volga discharge (average annual discharge is 240 km^3; Kosarev, 2005) allows avoiding its desiccation during sea level fall and limits inundation during sea level rise (Fig. 9a). On the contrary, the Ural delta retreats and advances during sea level changes are related to its substrate slope (Fig. 9b).

Concerning the south coast, they are two groups of wetlands. One is dominated by seawater interactions, i.e. Ghizil-Agaj, Turkmenbashy Bay, GB, Gomishan Lagoon. The other one is dominated by freshwater inputs, i.e., Anzali Lagoon, Bujagh, Amirkola and Fereydoon Kenar (Leontiev et al., 1977; Khorami Pour et al., 2015). The latter have limited seawater penetration or do not allow seawater penetration into the lagoons. Extensive freshwater usage for agricultural fields and hard engineering construction across rivers that changed hydrological regimes around those lagoons accelerate lagoon shrinking and desiccation. Rapid sea level fall enhanced freshwater outflow by not supporting surface water level and groundwater table stabilization. In the south coast, the extension of the GB in the west (Lapoo-Zaghmarz), Fereydoon Kenar and Amirkola acutely depend on freshwater inputs. The former group has free water exchange with the CS and experienced gain and loss in area directly caused by sea level fluctuations; and

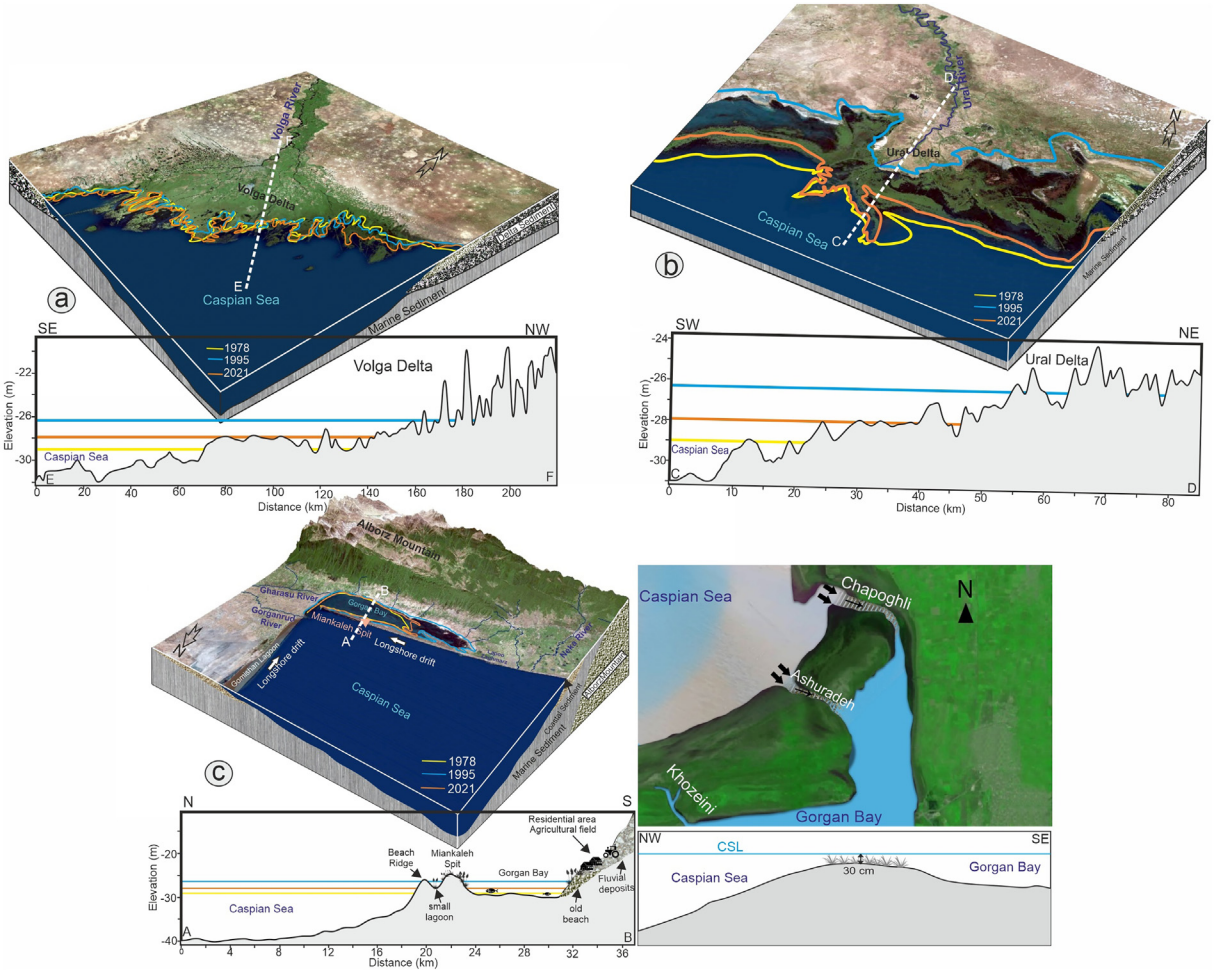

Fig. 9. Response of the Caspian coastal wetlands to CSL changes, horizontal lines: yellow, blue and orange correspond to sea level of 1978, 1995 and 2021 respectively. a) Volga Delta block diagram and a cross-section parallel to river axis, b) Ural Delta block diagram and a cross-section parallel to river axis c) Gorgan Bay and a cross section perpendicular to the Miankaleh Spit and coastline. Lower right panel represent three inlets of the Gorgan Bay with one of them desiccated and the two others shallower. At the bottom right, a cross section (not to scale) shows the very shallow entrance of the Gorgan Bay that requires to be deepened for better water exchange.

they never desiccated during the period of instrumental measurement. If the sea level fall had been in the same range as it was in the past few centuries, they would have undergone shrinking (Fig. 9c). Their desiccation depends on the inlet bottom level that permits water exchange between the bay/lagoon and the CS; and CSL has fluctuated by >3 m in the last centuries (e.g. Leroy et al., 2022a).

5.2. Gorgan Bay data

The GB water physical properties are affected by the adjacent CS waters and climate of the region. Dominant arid climate and lack of riverine flow affect seawater salinity in the Caspian eastern part (Kosarev, 2005). Accordingly, the CS surface water salinity is depended on the riverine inflow and climate of the region, which increases from west to east (Tuzhilkin and Kosarev, 2005; Kosarev, 2005). Climate around the GB changes from Mediterranean to semiarid. Salinity in the GB in our measurements shows a maximum of 20 Practical Salinity Scale that is much higher than the adjacent CS waters (Leroy et al., 2018). Salinity of the Caspian bays and lagoons changes from hypersaline in the east (Kara Bogaz Gol) and close to freshwater in the south west (Anzali Lagoon) (Terziev et al., 1996; Lahijani et al., 2008). In the shallow water of the GB, the water column is well mixed and has little vertical changes in salinity and temperature. Changes in electrical conductivity (salinity) in the inlet can be a criterion for detecting water exchange between the CS and GB. Due to the significant decrease in river discharge in the summer season and the increase in evaporation due to an increase in air temperature, an increase in electrical conductivity can be an indicator for the penetration of the GB water into the CS and a decrease in electrical conductivity indicates the influx of CS water into GB. Water deficit due to high evaporation compensated by the CS water that are visible in currents into the GB in Fig. S8 and S9.

Bacillariophyta was the dominant phytoplankton phylum and had the highest number of genera in the GB. Diatoms are considered euryhaline and eurythermal phytoplankton growing in moderate to high nutrient levels (Huang et al., 2004; Hubble and Harper, 2002). In this study, based on the ranges of temperature and salinity these conditions are classified as mesotrophic to eutrophic (Organization for Economic Cooperation and Development (OECD), 1982). A literature survey revealed similar results in other lagoons and wetlands in the Caspian Sea (Ganjian et al., 2010; Roohi et al., 2010; Nasrollahzadeh et al., 2008a, 2008b). Generally, the number of taxa increases from the west to east of the southern Caspian Sea (Kideys et al., 2008) as it is composed of 27 genera (12 diatoms) in the western coastal water (Bagheri et al., 2011) and increased to 68 genera (20 diatoms) in Miankaleh wetland in the east (Masoudi et al., 2012). This study presents temporal and spatial variations of phytoplankton composition in the GB and how the environmental conditions affect these variations. Results from this study show the phytoplankton composition in the bay is closely affected by the input of water from the CS and rivers along with the dynamics of physical conditions within the bay. These variations were controlled by nutrients, salinity and temperature. Nutrient availability was controlled by freshwater input and decomposition of organic material

within the bay, and salinity was controlled by relative importance of river discharge and currents from the CS. In addition, the sediment type is also affected by the accumulation of organic material (Mazaheri Kouhanestani et al., 2019). The average dissolved inorganic nitrogen in spring and summer was 24.5 and 16.7 micromolar respectively, which is higher than the eutrophication threshold (EPA, 1990). However, average dissolved inorganic phosphorus is around 0.5 micromolar which falls in normal condition.

Copepoda is the most important group of zooplankton in the CS (Raeiji et al., 2019) and according to other studies, it is also the most abundant in seas and in estuaries (Mauchline, 1998; Muxagata et al., 2012). The results of this research are similar to other researches in aquatic ecosystems (Ekwu and Sikoki, 2005; Davies et al., 2002; Kolo et al., 2003).

Compared to other sensitive coastal ecosystems in the south of the CS, such as the Anzali wetland, the dominance of Copepoda is also observed (Raeiji et al., 2019). In general, after the arrival of the invasive *Mnemiopsis leidyi* to the CS from the Black Sea, the species composition and abundance of zooplankton in the Caspian Sea and all aquatic ecosystems were affected and underwent many changes (Mohamadkhani and Gholampour, 2016).

5.3. Gorgan Bay simulations

The general water circulation in the GB is mainly controlled by atmospheric forcing, river input and the CSL. Our studies show that atmospheric forcing in water circulation acts through evaporation and wind, both of which have a main role also in homogenising water column. Simulation in different scenarios indicates higher water exchange during sea level rise and when inlets are wider and deeper. Also, residence time is reduced in enhanced water circulation. Results of previous numerical modelling in the area revealed that the GB water belongs to the barotropic type and that its general circulation is counter-clockwise annually (Ranjbar and Hadjizadeh Zaker, 2016). Our extensive measurements and simulations demonstrated the well mixed water mass (barotropic). However, our higher resolution study in circulation pattern shows counter-clockwise and clockwise patterns in different parts of the bay and in different seasons. Moreover, current velocity and speed data in the shallow and narrow inlet of the GB for the first time significantly improved our knowledge about water exchange that previously was based on simulation with scarce low-resolution measurements out of the inlets (Ranjbar and Hadjizadeh Zaker, 2016). In the current sea level fall, we proposed dredging of three inlets (Chapoghli, Ashuradeh and Khozeini) down to two meters depth and on a width of 200 m, as our simulation confirmed an enhancement of water exchange. Dredging would largely eliminate the *Ruppia maritima* areas in the inlets. These aquatic plants provide an ecosystem in themselves with associated services. Fortunately, they are enough seagrass meadows in other parts of the GB. The development of water exchange between wetland and main water body improves the abiotic water quality; however, the improvement of some biotic elements takes time to response to new condition (Wijnhoven et al., 2010; García-Oliva et al., 2019). The GB inlet maintenance follows two main goals, enhancement of the ecosystem functioning and the prevention from desiccation. We observed high sedimentation rates in our measurements in the GB inlet, which are comparable to the Caspian coastal lagoons and deltas (Leroy et al., 2011; Hoogendoorn et al., 2005; Lahijani et al., 2018). The CSL fall and high sedimentation rates could lead to the disconnection of GB from the CS. GB has 690 mmy^{-1} evaporation more than precipitation suggesting that, without CS waters, the GB will desiccate within two years. Wetlands desiccation around the CS (such as in the Aral Sea basin) caused a large increase in dust emission (Xi and Sokolik, 2016). Elguindi et al. (2016) simulated dust in the Caspian Sea region using RegCM4 model coupled with a one-dimensional lake model that showed the Karakum desert in Turkmenistan and the Kyzylkum desert in Uzbekistan around the Aral Sea are the main sources of dust storms in that region. The current simulation of dust in the GB area indicate that dust could expand up to 60 km with a concentration of 3500 μgkg^{-1}-dry air (Fig. S 11). Dust emission in residential area adversely impact on human health as dust in an agricultural area is heavily loaded with fertilizers and other pollutants (Goudie, 2014).

6. Discussion

6.1. Caspian Sea level and response of Caspian coastal Ramsar sites

The two north Caspian deltaic wetlands have important roles in ecosystem services. The Volga Delta is affected by ecosystem disturbances both from its catchment and in its delta itself; however, the Ural Delta is less affected by human activities (Lagutov, 2008; Leummens, 2018). The north Caspian wetlands support migratory birds, Caspian seals, the reproduction of fishes in particular endangered sturgeon species (Veshchev, 2009; Hoyt, 2022; Lagutov, 2008). Catchment and coastal management are implemented in deltaic wetlands to reduce stressors and restore ecosystem functioning (Cui et al., 2009; Day et al., 2019; Zhou et al., 2017). The effective management of the coastal zone as well as the catchment basins of Volga and Ural could reduce man-made stressors and allow the north Caspian wetlands to adapt to the challenging speed of CSL fluctuations (Lagutov, 2008; Leummens, 2018).

Unlike many deltaic wetlands that have lost area owing to intensive human activities (Wang et al., 2012; Coleman et al., 2008a, 2008b), the north Caspian wetlands are benefiting from being located in low density population coast.

In the south coast the west group of wetlands are under drastic shrinkage and deterioration, which requires management measures for rehabilitation (Khorami Pour et al., 2015; Sadeghi Zadegan, 2018a, 2018b; Bagherzadeh Karimi, 2018). They are coastal lagoons and bays. Different processes are attributed to the Caspian coastal lagoon/bay formation which include inundation of lowlands behind beach ridges due to rapid sea level rise, water penetration into lowlands in curved (geological synclines and anticlines) coastal areas, and engulfing coastal waters by enlargement of bars and spits (Leontiev et al., 1977; Kaplin and Selivanov, 1995; Kroonenberg et al., 2000). All south Caspian Ramsar sites were formed since the Neocaspian sea level rise with a strong littoral drift forming bars and spit enclosing some parts of coastal waters (Leontiev et al., 1977; Lahijani et al., 2009; Haghani and Leroy, 2016; Naderi Beni et al., 2013; Kakroodi et al., 2012). Protection and restoration of coastal wetlands have a positive impact on the ecosystem services that they provide (Wijnhoven et al., 2010; Zhang et al., 2021). The freshwater-dominated south Caspian Ramsar sites are located on the Iranian shores that are densely populated and attracts internal tourists during vacations (Pak and Farajzadeh, 2007; Alipour et al., 2017). Among seawater-dominated south Caspian Ramsar sites, Ghizil-Agaj in Azerbaijan and Turkmenbashy Bay in Turkmenistan have free water connection with the CS; however, Gomishan Lagoon in Iran is desiccated, and the GB has limited water connection. Despite of a surface area reduction in the current CSL fall, the Ghizil-Agaj and Turkmenbashy Bay wetland area individually are much larger than the total Caspian Ramsar sites in Iran. The small Caspian Ramsar sites in Iran are surrounded by densely populated area, and undergo extensive anthropogenic disturbances that are superimposed on the current CSL drop which lead to wetland loss and reduction in ecosystem services (Alipour et al., 2017; Pak and Farajzadeh, 2007; Khorami Pour et al., 2015).

The GB surface area was reduced by 40 % comparing to the 1995 area. The Miankaleh Spit has a strong littoral drift that causes its eastward growth, which leads to sediment deposition in the shallow inlets (Lahijani et al., 2009; Kakroodi et al., 2012). The GB inlets suffered from depth shallowing by current CSL fall at a rate of around 8 cmy^{-1} since 1996 and had an average sedimentation rate of 1.5 cmy^{-1}. Now aquatic plants especially seagrasses, grow in the inlets, which prevent free water exchange and trap more sediment for deposition. Measurement and simulation indicate a slow velocity of water exchange in the GB inlet, the main forcing of which is wind. In general, increased seawater exchange improves wetland water quality and assists wetland restoration (Eagle et al., 2022; Wijnhoven et al., 2010; Seiler et al., 2020). Climate and hydrology of the GB indicate that evaporation is twice the amount of precipitation and that riverine influx is limited due to intensive withdrawal. This shows that water deficit should be compensated from the CS. Our measurements as

well as previous measurements demonstrate that the GB water has elevated salinity comparing to the adjacent CS waters (Habibi, 2013; Leroy et al., 2018). According to the OECD classification, these conditions are classified as mesotrophic to eutrophic (OECD, 1982), and indeed this has been observed in the GB. This trend has been mentioned before in the GB (Aghili et al., 2018) and in the south CS coastal waters (Ganjian et al., 2010; Roohi et al., 2010; Nasrollahzadeh et al., 2008a, 2008b). In mesotrophic waters, the production of phytoplankton increases in terms of food supply and the depth of light penetration decreases. Simulation of water circulation have shown significant increase in the water exchange between the GB and the CS, which could dilute pollution and maintain wetland area to the level of the CS. Maintenance of the GB inlets would play a crucial role in GB ecosystem functions (Fig. 9c), because otherwise high sedimentation in the inlets, sea level fall and eastward growth of the Miankaleh Spit could isolate the GB from the CS that could lead to total desiccation. Simulation of dust emission shows that the GB could be a dust source in case of desiccation. The region experienced dust events in the past and desertification and wetland desiccation accelerate dust emission in the region (Honardoust et al., 2011; Elguindi et al., 2016; Rahimzadeh et al., 2019). Modelling of dust emission in Central Asia and the Aral Sea regions demonstrated that the Aral Sea desiccation and agricultural land use contribute to dust emission. The share of Aral Sea desiccation and agricultural land use in dust emission vary from 18 to 56 % using different dust schemes (Xi and Sokolik, 2016).

6.2. Restoration measures to mitigate the impact of sea level fall

A rapid assessment of three Ramsar sites on the south coast (Bujagh, Anzali and GB) demonstrates that they have shifted from normal conditions to deteriorated conditions with however a potential for restoration (Khorami Pour et al., 2015). Despite the higher current sea level compared to that of 1977, the wetlands encounter more stress caused by an exacerbated combination of both warming and anthropogenic impacts. Different actions should be taken to protect the coastal community and coastal ecosystems against the adverse effects of climate change and sea level extreme drop. Specific practices are considered for the most vulnerable areas and imminent threats. They include water allocation and prevention of inlet sedimentation. Water resources management and integrated coastal zone management for saving coastal ecosystems by domestic approaches are the main efforts at the national level. Based on our simulations and measurements in the GB, dredging of inlets on a 2 m depth and a 200 m width will enhance water exchange between the GB and the CS (Fig. 9c and Fig. S13). Inlet maintenance will improve water quality and prevent the GB from desiccation caused by CSL changes, as observed during the past centuries. In general, more water exchange of the coastal wetlands with the main water body improves the wetlands water quality (García-Oliva et al., 2019; Zainol et al., 2021). The restoration of the coastal wetland in the Dutch Delta improved significantly the wetland ecosystem with an artificially maintained water level (Wijnhoven et al., 2010).

National and regional efforts are needed to protect the CS from the harmful effects of climate change. As the CS is shared by the five rim countries of Iran, Turkmenistan, Kazakhstan, Russia and Azerbaijan, more political coordination is needed to conduct adaptation plans for the region. These collaborations should target first of all data and information exchange and joint managerial practices in the water body. An integrated coastal zone management promotes sustainable coastal development by adopting the use of natural resources in a way that avoids serious damage to the natural environment.

7. Conclusion

In the current research, we have investigated the impact of the CSL changes on the Caspian coastal wetlands that are registered as Ramsar sites. Aligned with the inter-comparison of these wetlands, we have focused on a possible restoration of the GB in the south-east corner of the CS using measurements and simulations. The mapping shows that the surface area of the Caspian coastal wetlands that are covered by the Caspian waters (excluding Fereydoon Kenar) is 9745, 13,413 and 9810 km^2 in the sea levels of 1978, 1995 and 2021 respectively. Despite the higher current sea level compared to 1978, the total surface area of the coastal wetlands has already fallen to the same level. Moreover, impacts significantly vary in the wetlands located in the densely populated south Caspian coast where wetlands loss and desiccation are more noticeable. The Volga Delta, receiving a significant influx of freshwater, compensates partially the current range of sea level drop and this situation partially protects it from wetland loss. The GB in the south Caspian coast encounters very limited water exchange with the CS due to shallowed inlets with the CSL fall, the enlargement of the Miankaleh Spit, sea grass extension and high sedimentation rate. Dust simulations have shown that in case of desiccation, it would become a local dust source for the adjacent area. Water circulation simulations proved that the deepening of the inlets could maintain water exchanges between the GB and the CS, which will improve water quality. Inlet deepening will restore the GB within a CSL change of a range that was experienced during the period of instrumental measurements. If the CSL drops more than what happened during the past century, all south Caspian Ramsar sites would face desiccation. Moreover, the north Caspian Ramsar sites encounter significant restrictions. Restoration measures would improve wetland condition, but more durable result requires management beyond the GB, i.e., in the catchment and coastal area for reducing human pressure. A limited literature is devoted to the internationally valuable Caspian Ramsar sites, much more efforts is needed to attract attentions to the devastating condition of the Caspian wetlands loss.

CRediT authorship contribution statement

Hamid A. K. Lahijani: Supervision, Conceptualization, Investigation, Writing – original draft, Resources. Jafar Azizpour: Investigation, Data analysis, Simulation, Validation, Writing. Klaus Arpe: Investigation, Data analysis, Simulation, Validation, Writing, Review & editing. Parvin Ghafarian: Data analysis, Simulation, Writing, Behrooz Abtahi: Investigation, Validation, Formal analysis, Resources, Project administration. Reza Rhanama: Investigation, Analysis, Writing – review & editing. Mohammad Ali Hamzeh: Investigation, Data analysis Writing. Ali Hamzehpour: Investigation, Formal analysis, Data quality control, Writing. Mohammadreza Mohammadpour: Simulation, Writing. Masoud Mahmoudof: Data analysis.

Data availability

The authors do not have permission to share data.

Declaration of competing interest

The authors declare that they have no known competing financial interests or personal relationships that could have appeared to influence the work reported in this paper.

Acknowledgement

This study has been supported by the Governorship of Golestan Province, Iran, through a research project, number 30107912-75. It was also partially supported by the Iranian National Institute for Oceanography and Atmospheric Science through a research project, number INIOAS-1400-012-01-02-01. Authors are deeply appreciative of Prof. S. Leroy who corrected the English of the manuscript and for her valuable suggestions to improve the paper.

Appendix A. Supplementary data

Supplementary data to this article can be found online at https://doi.org/10.1016/j.scitotenv.2022.158833.

References

Aali, R., Shahryari, A., 2021. Ecological problems of Gorgan Bay in the southeast corner of the Caspian Sea (Iran) and ways of improvement. J. Environ. Health Sustain. Dev. 7 (1), 1522–1524.

Aghili, K., Aghaye-Moghadam, A., Aghili, S.M., 2018. Study of trophic level of Gorgan Bay. J. Aquatic. Caspian Sea 3 (1), 55–62 in Persian.

Akhmadiyeva, Z., Abdullaev, 2019. Water management paradigm shifts in the Caspian Sea region: review and outlook. J. Hydrol. 568, 997–1006.

Alipour, H., Hossein, Olya, G.T., Hassanzadeh, B., Rezapouraghdam, H., 2017. Second home tourism impact and governance: evidence from the Caspian Sea region of Iran. Ocean. Coast. Manag. 136, 165–176.

Arpe, K., Leroy, S., 2007. The Caspian Sea level forced by the atmospheric circulation, asobserved and modelled. Quat. Int. 173–174, 144–152.

Arpe, K., Leroy, S.A.G., Lahijani, H., Khan, V., 2012. Impact of the european Russia drought in 2010 on the Caspian Sea level. Hydrol. Earth Syst. Sci. 16, 19–27. https://doi.org/10.5194/hess-16-19-2012.

Arpe, K., Leroy, S.A.G., Wetterhall, F., Khan, V., Hagemann, S., Lahijani, H., 2013. Prediction of the Caspian Sea level using ECMWF seasonal forecasts and reanalysis. Theor. Appl. Climatol. https://doi.org/10.1007/s00704-013-0937-6.

Arpe, K., Tsuang, B.-J., Tseng, Y.-H., Liu, X.-Y., Leroy, S.A.G., 2019. Quantification of climatic feed-backs on the Caspian Sea level variability and impacts from the Caspian Sea on the large scale atmospheric circulation. Theor. Appl. Climatol. 136 (1–2), 475–488.

Arpe, K., Molavi-Arabshahi, M., Leroy, S.A.G., 2020. Wind variability over the CaspianSea, its impact on Caspian seawater level and link with ENSO. Int. J. Climatol. 40 (14), 6039–6054. https://doi.org/10.1002/joc.6564.

Bagheri, S., Mansor, M., Makaremi, M., Sabkara, J., Maznah, W.O.W., Mirzajani, A., Khodaparast, S.H., 2011. Fluctuations of phytoplankton community in the coastal waters of Caspian Sea in 2006. Am. J. Appl. Sci. 8 (12), 1328–1336.

Bagherzadeh Karimi, M., 2018. Anzali mordab complex (Islamic Republic of Iran). In: Finlayson, C., Milton, G., Prentice, R., Davidson, N. (Eds.), The Wetland Book. Springer, Dordrecht.

Barale, V., 2008. The European and marginal seas: an overview. In: Barale, V., Gade, M. (Eds.), Remote Sensing of the European Sea. Springer, the Netherlands, pp. 3–22.

Chen, C., Cowles, G., Beardsley, R., 2006. An UnstructuredGrid, Finite-volume Coastal Ocean Model: FVCOM User Manual, SMAST/UMASSD.

Chen, C.H., Liu, R.C., Beardsley, 2003. An unstructured, finite-volume, three-dimensional, primitive equation ocean model: application to coastal ocean and estuaries. J. Atmos. Oceanic Tech. 20, 159–186.

Chen, J.L., Pekker, T., Wilson, C.R., Tapley, B.D., Kostianoy, A.G., Cretaux, J.F., Safarov, E.S., 2017. Long term Caspian sea level change. Geophys. Res. Let. 44 (13). https://doi.org/10.1002/2017GL07395.

Codiga, D.L., 2011. Unified Tidal Analysis and Prediction Using the UTide Matlab Functions. Technical Report 2011-01. Graduate School of Oceanography, University of Rhode Island, Narragansett, RI.

Coleman, J.M., Huh, O.K., Jr, DeWitt Braud, D., 2008a. Wetland loss in world deltas. J. Coast. Res. 24 (sp1), 1–14. https://doi.org/10.2112/05-0607.1.

Coleman, James M., Huh, Oscar K., Jr, DeWitt Braud, 2008b. Wetland loss in world deltas. J. Coast. Res. 24, 1–14.

Cui, B., Yang, Q., Yang, Z., Zhang, K., 2009. Evaluating the ecological performance of wetland restoration in the Yellow River delta, China. Ecol. Eng. 35, 1090–1103.

Davies, O.A., Inko-Tariah, M.B., Aririsukwu, N.U., 2002. Distribution of plankton populations in Elechi Creek (Eagle Island) Niger Delta. Zoology International Conference, Jan 14-18th 2002, Ibadan.

Day, J.W., Craig, C., Kemp, G.P., 2019. b. Mississippi Delta restoration and protection: shifting baselines, diminishing resilience, and growing nonsustainability. In: Wolanski, E., Day, J., Elliott, M., et al. (Eds.), Coasts and Estuaries: The Future. Elsevier, Waltham, MA, pp. 167–186.

Dee, D.P., Uppala, S.M., Simmons, A.J., Berrisford, P., Poli, P., Kobayashi, S., Andrae, U., Balmaseda, M.A., Balsamo, G., Bauer, P., Bechtold, P., Van De Berg, L., Bidlot, J., Bormann, N., Delsol, C., Dragani, R., Fuentes, M., Geer, A.J., Haimberger, L., Healy, S.B., Hersbach, H., Hólm, E.V., Isaksen, L., Kållberg, P., Köhler, M., Matricardi, M., McNally, A.P., Monge-Sanz, B.M., Morcrette, J.J., Park, B.K., Peubey, C., de Rosnay, P., Tavolato, C., Thépaut, J.N., Vitart, F., Beljaars, A.C.M., 2011. The ERA –interim reanalysis: configuration and performance of the data assimilation system. Quart. J. Roy. Meteorol. Soci 137 (656), 553–597. https://doi.org/10.1002/qj.828.

Demin, A.P., 2007. Present-day changes in water consumption in the Caspian Sea basin. Water Resour. 34, 237–253.

Derolez, V., Malet, N., Fiandrino, A., Lagarde, F., Richard, M., Ouisse, V., Bec, B., Aliaume, C., 2020. Fifty years of ecological changes: regime shifts and drivers in a coastal Mediterranean lagoon during oligotrophication. Sci. Tot. Environ. 732.

Eagle, M.J., Kroeger, K.D., Spivak, A.C., Wang, F., Tang, J., Abdul-Aziz, O.I., Ishtiaq, K.S., O'Keefe, S.J., Mann, A.G., 2022. Soil carbon consequences of historic hydrologic impairment and recent restoration in coastal wetlands. Sci. Total Environ. 848, 157682.

ECMWF-ERA, 2018. Available at https://www.ecmwf.int/forecasts/datasets/archive-Datasets. https://www.ecmwf.int/en/forecasts/datasets/browsereanalysis-datasets (Accessed November 2018).

Ekwu, A.O., Sikoki, F.D., 2005. Preliminary checklist and distribution of zooplankton in the lower Cross River Estuary. Fisheries Society Conference. 14th – 18th November 2005, Port Harcourt.

Elguindi, N., Giorgi, F., 2006. Projected changes in the Caspian Sea level for the 21st century based on the latest AOGCM simulations. Geophys. Res. Lett. 33, 4–7.

Elguindi, N., Solmon, F., Turuncoglu, U., 2016. Quantifying some of the impacts of dust and other aerosol on the Caspian Sea region using a regional climate model. Clim. Dyn. 46, 41–55.

Emery, W.J., Thomson, R.E., 2004. Data analysis methods. Physical Oceanography, 2edn Elsevier BV, New Yok.

EPA, 1990. Nutrients in European ecosystems. Environmental Assessment Report No. 4 155p.

Fan, J., Wang, X., Wu, W., Chen, W., Ma, Q., Ma, Z., 2021. Function of restored wetlands for waterbird conservation in the Yellow Sea coast. Sci. Total Environ. 756, 144061.

Forte, A.M., Cowgill, E., 2013. Late cenozoic base-level variations of the Caspian Sea: a review of its history and proposed driving mechanisms. Palaeogeogr. Palaeoclimatol. Palaeoecol. 386, 392–407.

Frolov, A.V., 2003. Modeling of the Long-term Fluctuations of the Caspian Sea Level; Theory and Applications. GEOS, Moscow 172 p.

Ganjian, A., Wan Maznah, W.O., Yahya, K., Fazli, H., Vahedi, M., Roohi, A., Farabi, S.M.V., 2010. Seasonal and regional distribution of phytoplankton in the southern part of the Caspian Sea. Iran. J. Fish. Sci. 9, 382–401.

García-Oliva, M., Marcos, C., Umgiesser, G., McKiver, W., Ghezzo, M., De Pascalis, F., Pérez-Ruzafa, A., 2019. Modelling the impact of dredging inlets on the salinity and temperature regimes in coastal lagoons. Ocean Coast. Manag. 180 (2019), 104913. https://doi.org/10.1016/j.ocecoaman.2019.104913.

Gaybullaev, B., Chen, S.C., Kuo, Y.M., 2012. Large-scale desiccation of the Aral Sea due to over-exploitation after 1960. J. Mt. Sci. 9, 538–546.

Gholizadeh, M., Cera, A., 2022. Microplastic contamination in the sediments of Qarasu estuary in Gorgan Bay, south-east of Caspian Sea, Iran. Sci. Tot. Enviro. 838 (1), 155913.

Goodman, S., Dmitrieva, L., 2016. Pusa caspica. The IUCN Red List of Threatened Species. 2016. https://doi.org/10.2305/IUCN.UK.20161.RLTS.T41669A45230700.en e. T41669A45230700.

Goudie, A.S., 2014. Desert dust and human health disorders. Environ. Int. 63, 101–113.

Grasshoff, K.K., Ehrhardt, M., 1999. Methods of Seawater Analysis. Third ed. 632. John Wiley & Sons.

Grell, G.A., Peckham, S.E., Schmitz, R., McKeen, S.A., Frost, G., Skamarock, W.C., Eder, B., 2005. Fully coupled "online" chemistry within the WRF model. Atmos. Environ. 39 (37), 6957–6975. https://doi.org/10.1016/j.atmosenv.2005.04.027.

Grenfell, S.E., Callaway, R.M., Grenfell, M.C., Bertelli, C.M., Mendzil, A.F., Tew, I., 2016. Will a rising sea sink some estuarine wetland ecosystems? Sci. Total Environ. 554–555 (2016), 276–292.

Habibi, P., 2013. Distribution,Diversity and Morphology of Holocene Benthic Foraminifera Assemblage of theGolestan Coast. MSc thesis. Payam Noor University, Tehran 116p. (In Persian).

Haghani, S., Leroy, S.A.G., 2016. Differential impact of long-shore currents on coastal geomorphology development in the context of rapid sea level changes: the case of the old sefidrud (Caspian Sea). Quat. Int. 408, 78–92.

Haghani, S., Leroy, S.A.G., 2020. Recent avulsion history of sefidrud, south west of the Caspian Sea. Quat. Int. 540, 97–110.

Heiri, O., Lotter, A., Lemcke, G., 2001. Loss on ignition as a method for estimating organic and carbonate content in sediments: reproducibility and comparability of results. J. Paleolim. 25, 101–110.

Honardoust, F., Ownegh, M., Sheikh, V., 2011. Assessing desertification sensitivity in the northern part of Gorgan plain, southeast of the Caspian Sea. Iran. Res. J. Environ. Sci. 5, 205.

Hoogendoorn, R.M., Boels, J.F., Kroonenberg, S.B., Simmons, M.D., Aliyeva, E., Babazadeh, A.D., Huseynov, D., 2005. Development of the kura delta, Azerbaijan; a record of holocene Caspian Sea-level changes. Mar. Geol. 222–223, 359–380. https://doi.org/10.1016/j.margeo.2005.06.007.

Hoyt, E., 2022. Habitats of the endangered Caspian seal identified as important marine mammal areas. Oryx 56 (2), 170–171.

Huang, L., Jian, W., Song, X., Huang, X., Liu, S., Qian, P., Yin, K., Wu, M., 2004. Species diversity and distribution for phytoplankton of the Pearl River estuary during rainy and dry seasons. Mar. Pollut. Bull. 49 (7–8), 588–596. https://doi.org/10.1016/j.marpolbul.03.015.

Hubble, D.S., Harper, D.M., 2002. Phytoplankton community structure and succession in the water column of Lake Naivasha, Kenya: a shallow tropical lake. Hydrobio. 488 (1/3), 89–98. https://doi.org/10.1023/A:1023314128188.

IPCC, 2013. In: Stocker, T.F., Qin, D., Plattner, G.-K., Tignor, M., Allen, S.K., Boschung, J., Nauels, A., Xia, Y., Bex, V., Midgley, P.M. (Eds.), Climate Change 2013: The Physical Science Basis. Contribution of Working Group I to the Fifth Assessment Report of the Intergovernmental Panel on Climate Change. Cambridge University Press, Cambridge, United Kingdom and New York, NY, USA 1535 pp.

Janse, J.H., Van Dam, A.A., Hes, E.M.A., de Klein, J.J.M., Finlayson, C.M., Janssen, A.B.G., Wijk, D.V., Mooij, W.M., Verhoeven, J.T.A., 2019. Towards a global model for wetlands ecosystem services. Curr. Opin. Environ. Sustain. 36, 11–19.

Kakroodi, A.A., Kroonenberg, S.B., Hoogendoorn, R.M., MohammdKhani, H., Yamani, M., Ghassemi, M.R., Lahijani, H., 2012. Rapid Holocene sea-level changes along the Iranian Caspian coast. quarterInter. 263, 93–103.

Kakroodi, A.A., Leroy, S.A.G., Kroonenberg, S.B., Lahijani, H.A.K., Alimohammadian, H., Boomer, I., Goorabi, A., 2015. Late pleistocene and Holocene Sea-level change and coastal palaeoenvironment evolution along the iranian Caspian shore. Mar. Geol. 361, 111–125.

Kaplin, P.A., Selivanov, A.O., 1995. Recent coastal evolution of the Caspian Sea as a natural model for coastal responses to the possible acceleration of global sea-level rise. Mar. Geol. 124, 161–175.

Karydis, M., 2009. Eutrophication assessment of coastal waters based on indicators: a literature review. Glob. Nest J. 11 (4), 373–390.

Khorami Pour, S., Monavari, S.M., Riazi, B., Khorasani, N., 2015. Caspian rapid assessment method: a localized procedure for assessment of wetlands at southern fringe of the Caspian Sea. Environ. Monit. Assess. 187 (7), 420.

Kideys, A.E., Roohi, A., Eker-Develi, E., Mélin, F., Beare, D., 2008. Increased chlorophyll levels in the southern Caspian Sea following an invasion of jellyfish. Res. Lett. Ecol. 2008, 1–4. https://doi.org/10.1155/2008/185642.

Kolo, R.J., Mani, I.A., Musa, H.A., 2003. Effects of different types of fertilizers on plankton productivity in earthen ponds. 16th Annual Conference of the Fisheries Society of Nigeria (FISON) 4–9 November 2001. Maiduguri, Nigeria, pp. 127–131.
Kopelevich, O.V., Burenkov, V.I., Ershova, S.V., Sheberstov, S.V., Evdoshenko, M.A., 2004. Application of SeaWiFS data forstudying variability of bio-optical characteristics in the barents, black and Caspian seas. Deep-Sea Res. Pt. II 51, 1063–1091.
Koriche, S.A., Singarayer, J., Cloke, H., 2021. The fate of the Caspian Sea Under projectedclimate change and water extraction during the 21st century. Environ. Res. Lett. 16, 094024.
Koroleff, F., 1983. Determination of ammonium. In: Grasshoff, K., Ehrhardt, M., Kremling, K. (Eds.), Methods of Seawater Analysis. Verlag Chemic, pp. 150–157.
Kosarev, A.N., 2005. Physico-geographical conditions of the Caspian Sea. In: Kostianoy, A.G., Kosarev, A.N. (Eds.), The Caspian Sea Environment. Springer, Berlin, pp. 5–31.
Kozerski, H.P., 1994. Possibilities and limitations of sediment traps to measure sedimentation and resuspension. Hydrobiologia 284, 93–100.
Kroonenberg, S.B., Badyukova, E.N., Storms, J.E.A., Ignatov, E.I., Kasimov, N.S., 2000. A full sea-level cycle in 65 years: barrier dynamics along Caspian shores. Sed. Geol. 134, 257–274.
Lagutov, V., 2008. The Ural river basin: hydrology, characteristics and water use. In: Lagutov, V. (Ed.), Rescue of Sturgeon Species in the Ural River Basin. Environmental Security. Springer, Dordrecht, NATO Science for Peace and Security Series C.
Lahijani, H., Tavakoli, V., Amini, A., 2008. River mouth configuration in South Caspian Coast, Iran. Environ. Sci. 5, 65–86.
Lahijani, H., Rahimpour-Bonab, V.H., Tavakoli, M.Hosseindoost, 2009. Evidence for late Holocene highstands in Central Guilan- East Mazanderan, South Caspian coast, Iran. Quarter. Inter. 197, 55–71.
Lahijani, H., Leroy, S., Beni, M.N., Arpe, A., 2010. Blaze in Volga: Is it a critical point for the fall in Caspian Sea level? EPISO 33 (3) 208-208.
Lahijani, H., Abbasian, H., Naderi-Beni, A., Leroy, S.A., Habibi, P., Haghani, S., Hosseindost, M., Shahkarami, S., Yeganeh, S., Zandinasab, Z., Tavakoli, V., 2018. Sediment distribution pattern of South Caspian Sea: possible hydroclimatic implications. Can. J. Earth Sci. 56 (6), 637–653.
Lefebvre, G., Redmond, L., Germain, C., Palazzi, E., Terzago, S., Willm, L., Poulin, B., 2019. Predicting the vulnerability of seasonally-flooded wetlands to climate change across the Mediterranean Basin. Sci. Total. Environ. 692, 546–555.
Leontiev, O.K., Maev, N.G., Richagov, G.I., 1977. Geomorphology of the Caspian Coast and Sea. Moscow State. Univ. 208p.
Leroy, S., Lahijani, H., Djamali, M., Naginezhad, A., Moghadam, M., Arpe, K., Hosseindoust, M., Habibi, P., Naderi, M., Shah-hosseini, M., Ch, Miller, Tavakoli, V., 2011. Late Little Ice Age palaeoenvironmental records from the Anzali and Amirkola Lagoons (South Caspian Sea): Vegetation and Sea level changes. Palaeogeography, Palaeovlimatology, Palaeoecology 302, 415–434.
Leroy, S.A., Chalie, F., Wesselingh, F.P., Sanjani, M.S., Lahijani, H., Athersuch, J., Kabiri, K., 2018. Multi-proxy indicators in a pontocaspian system: a depth transect of surface sediment in the SE Caspian Sea. Geol. Belg. 21, 3–4.
Leroy, S.A.G., Amini, A., Gregg, M., Marinova, E., Bendrey, R., Zha, Y., Naderi Beni, A.M., Fazeli Nashli, H., 2019. Human responses to environmental changes on the southern coastal plain of the Caspian Sea during the Mesolithic and Neolithic periods. Quat. Sci. Rev. 218, 343–364.
Leroy, S.A.G., Reimer, P.J., Lahijani, H.K., Naderi Beni, A., Sauer, E., Chalié, F., Arpe, K., Demory, F., Mertens, K., Belkacem, D., Kakroodi, A.A., Omrani Rekavandi, H., Nokandeh, J., Amini, A., 2022a. Caspian Sea levels over the last 2200 years, with new data from the S-E corner. Geomorph 403 (15), 108–136.
Leroy, S.A.G., Gracheva, R., Medvedev, A., 2022b. Natural hazards and disasters around the Caspian Sea. Nat. Hazards https://doi.org/10.1007/s11069-022-05522-5.
Leroy, S.A.G., Demory, F., Chalié, F., Bates, R., Bates, M., Omrani Rekavandi, H., Sauer, E., 2022c. Palaeoenvironments at the Caspian terminals of the Gorgan and Tammisheh walls. Sauer et al. "Ancient Arms Race, Antiquity's Largest Fortresses and Sasanian Military Networks Of Northern Iran". The British Institute of Persian Studies, Archaeological Monographs Series VII13. Oxbow book, pp. 425–441 ISBN: 9781789254624.
Leummens, H.J.L., 2018. Volga river delta (Russia). In: Finlayson, C., Milton, G., Prentice, R., Davidson, N. (Eds.), The Wetland Book. Springer, Dordrecht.
Liu, L., Wang, H., Yue, Q., 2020. China's coastal wetlands: ecological challenges, restoration, and management suggestions. Reg. Stud. Mar. Sci. 37, 101337.
Maleki, P., Patimar, R., Jafariyan, H., Mahini, A.R., Ghorbani, R., Gholizadeh, M., Harsij, M., 2020. Ecological assessment of organic pollution in the Gorgan Bay, using palmer algal index. Iran. J. Appl. Ecol. 9 (1), 45–59.
Martin, D.M.Jacobs, Jacobs, A.D., McLean, C., Canick, M.R., Boomer, K., 2022. Comparing normative and descriptive methods for multi-criteria decision analysis: A case study evaluating wetland restoration opportunities in the Chesapeake Bay watershed, USA. Environ. Sci. Poli. 132, 142–152.
Masoudi, M., Ramezannejad, R., Riahi, H., 2012. Phytoplankton flora of miankaleh wetland. Iran. J. Bot. 18, 141–148. https://doi.org/10.22092/ijb.2012.13150.
Mauchline, J., 1998. The biology of calanoid copepods. Adv. Mar. Biol. 33, 1–170. https://doi.org/10.1038/179325a0.
Mazaheri Kouhanestani, Z., Roelke, D.L., Ghorbani, R., Fujiwara, M., 2019. Assessment of spatiotemporal phytoplankton composition in relation to environmental conditions of Gorgan Bay. Iran. Estuar. Coast. 42, 173–189. https://doi.org/10.1007/s12237-018-0451-2.
Mikhailov, V.N., 1997. River mouths of Russia and adjacent countries. GEOC, Moscow 444pp.
Mikhailov, V.N., Mikhailova, M.V., Isupova, M.V., 2014. Hydrological and morphological processes at river mouths of the Caspian Sea region as possible analogs of expected changes of mouths of other rivers in Russia and the world. Water Resour. 41, 489–504.
Miloshis, M., Fairfield, C.A., 2015. Coastal wetland management. A rating system for potential engineering interventions. Ecol. Eng. 75, 195–198.
Mohamadkhani, H., Gholampour, T., 2016. Zooplankton of south Caspian Sea (Gorgan Bay). J. New Tech. Aqua. Devel 11 (3), 39–46 in persian.
Murphy, J., Riley, J., 1962. A modified single solution for the determinationof phosphate in natural waters. Anal. Chim. Act. 27, 31–36.
Muxagata, E., Amaral, W.J.A., Barbosa, C.N., 2012. Acartia tonsa production in the Patos Lagoon estuary, Brazil. ICES J. Mar. Sci. 69, 475–482. https://doi.org/10.1093/icesjms/fsr166.
Naderi Beni, A., Lahijani, H., Moussavi Harami, R., Leroy, S.A.G., Shah-Hosseini, M., Tavakoli, V., Kabiri, K., 2013. Development of spit–lagoon complexes in response to Little Ice Age rapid sea-level changes in the central Guilan coast, South Caspian Sea, Iran. Geomorph. 187, 11–26.
Nandini-Weiss, S.D., Prange, M., Arpe, K., Merkel, U., Schulz, M., 2019. Past and future impact of the winter North Atlantic oscillation in the Caspian Sea catchment area. Int. J. Climatol. 40 (5), 2717–2731.
Narayan, S., Beck, M.W., Wilson, P., Thomas, C.J., Guerrero, A., Shepard, C.C., Reguero, B.G., Franco, G., Ingram, J.C., Trespalacios, D., 2017. The value of coastal wetlands for flood damage reduction in the northeastern USA. Sci. Rep. 7.
Nasrollahzadeh, H.S., Din, Z.B., Foong, S.Y., Makhlough, A., 2008a. Spatial and temporal distribution of macronutrients and phytoplankton before and after the invasion of the ctenophore, Mnemiopsis leidyi, in the southern Caspian Sea. Chem. Ecol. 24 (4), 233–246. https://doi.org/10.1080/02757540802310967.
Nasrollahzadeh, H.S., Bin Din, Z., Foong, S.Y., Makhlough, A., 2008b. Trophic status of the iranian Caspian Sea based on water quality parameters and phytoplankton diversity. Cont. Shelf Res. 28 (9), 1153–1165. https://doi.org/10.1016/j.csr.2008.02.015.
Nikolaeva, P.V., 1971. New morphometric characteristics of the Caspian Sea. MOIP Bull. 1. USSR. 143 pp
Organization for Economic Cooperation and Development (OECD), 1982. Eutrophication of Waters, Monitoring, Assessment and Control. OECD Publications, Paris.
Pak, A., Farajzadeh, M., 2007. Iran's integrated coastal management plan: persian gulf, Oman Sea, and southern Caspian Sea coastlines. Ocean Coast. Manag. 50, 754–773.
Prange, M., Wilke, T., Wesselingh, F.P., 2020. The other side of sea level change. Commun. Earth. Environ. 1, 69.
Raeiji, H., Gholizade, M., Patimar, R., Taher Pursofi, T., 2019. Investigating the density and frequency of zooplankton in the Southeastern Basin of the Caspian Sea (Gorgan Bay). Iran. Sci. Fish. J. 28 (2), 59–70 (in Persian).
Rahimzadeh, N., Khormali, F., Gribenski, N., Kiani, F., Frechen, M., 2019. Timing and development of sand dunes in the Golestan Province, northern Iran—Implications for the Late-Pleistocene history of the Caspian Sea. Aeolian Res. 41, 100538.
Ramsar Convention on Wetlands, 2021. In: Wetlands, R.C.O. (Ed.), The List of Wetlands of International Importance.
Ramsar List, 2020. The List of Wetlands of International Importance. 55 P. https://www.ramsar.org/.
Ranjbar, M.H., Hadjizadeh Zaker, N., 2016. Estimation of environmental capacity of phosphorus in Gorgan Bay, Iran, via a 3D ecological-hydrodynamic model. Environ. Monit. Assess. 188, 649.
Rashki, A., Middleton, N.J., Goudie, A.S., 2021. Dust storms in Iran -distribution, causes, frequencies and impacts. Aeolian. Res. 48, 100655.
Reed, D., Wang, Y., Meselhe, E., White, E., 2020. Modeling wetland transitions and loss in coastal Louisiana under scenarios of future relative sea-level rise. Geomorphology 352, 106991.
Renssen, H., Lougheed, B.C., Aerts, J.C.J.H., de Moel, H., Ward, P.J., Kwadijk, J.C.J., 2007. Simulating long-term Caspian Sea level changes: the impact of Holocene and future climate conditions, Earth Planet. Sci. Lett. 261 685-69.
Rodionov, S., 1994. Global and Regional Climate Interaction: The Caspian Sea Experience. Kluwer Academic Publications. Springer, New York.
Rolph, G., Stein, A., Stunder, B., 2017. Real-time environmental applications and display system. Environ. Model. Soft. 95, 210–228.
Roohi, A., Kideys, A.E., Sajjadi, A., Hashemian, A., Pourgholam, R., Fazli, H., Khanari, A.G., Eker-Develi, E., 2010. Changes in biodiversity of phytoplankton, zooplankton, fishes and macrobenthos in the southern Caspian Sea after the invasion of the ctenophore mnemiopsis leidyi. Biol. Invasions 12, 2343–2361. https://doi.org/10.1007/s10530-009-9648-4.
Rychagov, G.I., 1997. Holocene oscilliations of the Caspian Sea and forecasts based onpaleogeographicalreconstructions. Quat. Int. 41 (42), 167–172.
Sadeghi Zadegan, S., 2018a. Bujagh National Park (Islamic Republic of Iran). In: Finlayson, C., Milton, G., Prentice, R., Davidson, N. (Eds.), The Wetland Book. Springer, Dordrecht.
Sadeghi Zadegan, S., 2018b. Fereydoon Kenar, Ezbaran, and Sorkh Ruds Ab-Bandans. In: Finlayson, C., Milton, G., Prentice, R., Davidson, N. (Eds.), The Wetland Book. Springer, Dordrecht.
Seiler, L.M.N., Fernandes, E.H.L., Siegle, E., 2020. Effect of wind and river discharge on water quality indicators of a coastal lagoon. Reg. Stud. Mar. Sci. 40, 101513.
Sharifi, A., Shah-Hosseini, M., Pourmand, A., Esfahaninejad, M., Haeri-Ardakani, O., 2018. The vanishing of urmia Lake: a geolimnological perspective on the hydrological imbalance of the World's second largest hypersaline Lake. The Handbook of Environmental Chemistry. Springer, Berlin, Heidelberg.
Skamarock, W.C., Klemp, J.B., Dudhia, J., Gill, D.O., Liu, Z., Berner, J., Wang, W., Powers, J.G., Duda, M.G., Barker, D.M., Huang, X.Y., 2019. A Descriptionof the Advanced Research WRF Model Version 4. National Center for Atmospheric Research, Boulder, CO, USA, p. 145.
Spencer, T., Schuerch, M., Nicholls, R.J., Hinkel, J., Lincke, D., Vafeidis, A.T., Reef, R., McFadden, L., Brown, S., 2016. Global coastal wetland change under sea-level rise and related stresses: the DIVA wetland change model. Glob. Planet. Chang. 139, 15–30.
Stein, A.F., Draxler, R.R., Rolph, G.D., Stunder, B.J., Cohen, M.D., Ngan, F., 2015. NOAA's HYSPLIT atmospheric transport and dispersion modeling system. Bull. Amer. Meteorol. Soci. 96, 2059–2077.

Steyer, G., Llewellyn, D., 2000. Coastal wetlands planning, protection, and restoration act: aprogrammatic application of adaptive management. Ecol. Eng. 15, 385–395.
Szmytkiewicz, A., Zalewska, T., 2013. Sediment deposition and accumulation rates determined by sediment trap and 210Pb isotope methods in the outer Puck Bay (Baltic Sea). Oceanology 56, 85–106.
Terziev, S.F., Maksimova, M.P., Yalonsky, E.A., 1996. Hydrometeorology and Hydrochemistry of Seas, The Caspian Sea, Hydrochemical Conditions and Oceanological Principle in Formation of Biological Productivity. Gidrometeoizdat, Leningrad 322p.
Tuzhilkin, V.S., Kosarev, A.N., 2005. Thermohaline structure and general circulation of the Caspian Sea waters. In: Kostianoy, A.G., Kosarev, A.N. (Eds.), The Caspian Sea Environment. Springer, Berlin/Heidelberg, pp. 33–57.
UNESCO, 2022. https://en.unesco.org/biosphere/aspac/miankaleh.
Varushenko, S.I., Varushenko, A.N., Klige, R.K., 1987. Changing of the Caspian Sea Regime and Enclosed Basins in Geological Time, Moscow, Nauka, p. 240.
Vazin, N., 2021. Sustainable Communities: A Case Study of the Miankaleh Wetland, Iran. Sustainability and Climate Change Dec, 401–414.
Veshchev, P.V., 2009. The state of natural reproduction of stellate sturgeon Acipenser stellatus in the lower Volga. J. Ichth. 49, 662–667.
Voropaev, G.V., 1986. The Caspian Sea: Hydrology and Hydrochemistry. Nauka, Moscow, p. 262.
Wang, M., Qi, S., Zhang, X., 2012. Wetland loss and degradation in the Yellow River Delta, Shandong Province of China. Environ. Earth Sci. 67, 185–188.
White, J., 1990. The use of sediment traps in high energy environments. Mar. Geophys. Res. 12, 145–152.
Wijnhoven, S., Escaravage, V., Daemen, E., et al., 2010. The decline and restoration of a coastal lagoon (Lake Veere) in the Dutch Delta. Estuar. Coasts 33, 1261–1278.
Wood, E.D., Armstrong, F.A.J., Richards, F.A., 1967. Determination of nitrate in sea water by cadmium copper reduction to nitrite. J. Mar. Biol. Assoc. U. K. 47, 23–31.
Wu, W., Zhi, C., Gao, Y., Chen, C., Chen, Su, H., Lu, W., Tian, B., 2022. Increasing fragmentation and squeezing of coastal wetlands: status, drivers, and sustainable protection from the perspective of remote sensing. Sci. Total Environ. 811, 152339.
Xi, X., Sokolik, I.N., 2016. Quantifying the anthropogenic dust emission from agricultural land use and desiccation of the Aral Sea in Central Asia. J. Geophys. Res.-Atmos. 121, 12270–12281.
Xu, X., Chen, M., Yang, G., Jiang, B., Zhang, J., 2020. Wetland ecosystem services research: a critical review. Glob. Ecol. Conserv. 22, 1027.
Yuan, L., Liu, D., Tian, B., Yuan, X., Bo, S., Ma, Q., Wu, W., Zhao, Z., Zhang, L., Keesing, J.K., 2022. A solution for restoration of critical wetlands and water bird habitats in coastal deltaic systems. J. Environ. Manag. 15, 113996.
Zainol, Z., Akhir, M.F., Zainol, Z., 2021. Pollutant transport and residence time of a shallow and narrow coastal lagoon estimated using a numerical model. Mar. Pollut. Bull. 164, 112011.
Zhang, S., Zhang, P., Pan, B., Zou, Y., Xie, Y., Zhu, F., Chen, X., Li, F., Deng, Z., Zhang, H., Yang, S., 2021. Wetland restoration in the east dongting Lake effectively increased waterbird diversity by improving habitat quality. Glob. Ecol. Conserv. 27, 1535.
Zhou, R., Li, Y., Wu, J., Gao, M., Wu, X., Bi, X., 2017. Need to link river management with estuarine wetland conservation: a case study in the Yellow River Delta, China. Ocean. Coast. Manag. 146, 43–49.
Zucca, C., Middelton, N., Kang, U., Liniger, H., 2021. Shrinking water bodies as hotspots of sand and dust storms. The role of land degradation and sustainable soil and water management. Catena 207, 105669.